

Published in "Galactic and Extragalactic Radio Astronomy", 1988, 2nd edition, eds. G.L. Verschuur and K.I. Kellerman.

13. RADIO GALAXIES AND QUASARS

Kenneth I. Kellermann and Frazer N. Owen

Table of Contents

- [INTRODUCTION](#)
 - [Optical Counterparts](#)
 - [Radio Source Properties](#)
 - [Radio Spectra](#)
 - [Energy Considerations](#)

- [LOW-LUMINOSITY SOURCES](#)
 - [Spiral, Seyfert, and Irregular Galaxies](#)
 - [Elliptical Galaxies](#)

- [COMPACT SOURCES](#)
 - [Self-Absorption](#)
 - [Inverse Compton Radiation](#)
 - [Polarization](#)
 - [Structure](#)
 - [Variability](#)
 - [Source Dynamics and Superluminal Motion](#)
 - [Relativistic Beaming](#)

- [EXTENDED SOURCES](#)
 - [Jets, Lobes, and Hot Spots](#)
 - [Jet Physics](#)

- [SUMMARY](#)

- [REFERENCES](#)

13.1. INTRODUCTION

All galaxies and quasars appear to be sources of radio emission at some level. Normal spiral galaxies such as our own galactic system are near the low end of the radio luminosity function and have radio luminosities near 10^{37} erg s⁻¹. Some Seyfert galaxies, starburst galaxies, and the nuclei of active elliptical galaxies are 100 to 1000 times more luminous. Radio galaxies and some quasars are powerful radio sources at the high end of the luminosity function with luminosities up to 10^{45} erg s⁻¹.

For the more powerful sources, the radio emission often comes from regions well removed from the associated optical object, often hundreds of kiloparsecs or even megaparsecs away. In other cases, however, particularly in active galactic nuclei (AGN) or quasars, much of the radio emission comes from an extremely small region with measured dimensions of only a few parsecs. The form of the radio-frequency spectra implies that the radio emission is nonthermal in origin; it is presumed to be synchrotron radiation from ultra-relativistic electrons with energies of typically about 1 GeV moving in weak magnetic fields of about 10^{-4} gauss (see [Section 1.1](#)).

The extended radio sources constitute the largest known physical structures in the universe. Their energy content is very large, up to 10^{60} erg or more. The origin of this energy and the manner in which it is converted into relativistic particles and magnetic fields has remained one of the most challenging problems of modern astrophysics. High-resolution radio images generally show a very compact component which is coincident with an active galactic nucleus or quasar, and which is thought to reflect the "central engine." Long thin "jets" extend away from the compact central core toward the outer radio lobes. Often the jets end up at *hot spots* ([Figure 13.1](#)).

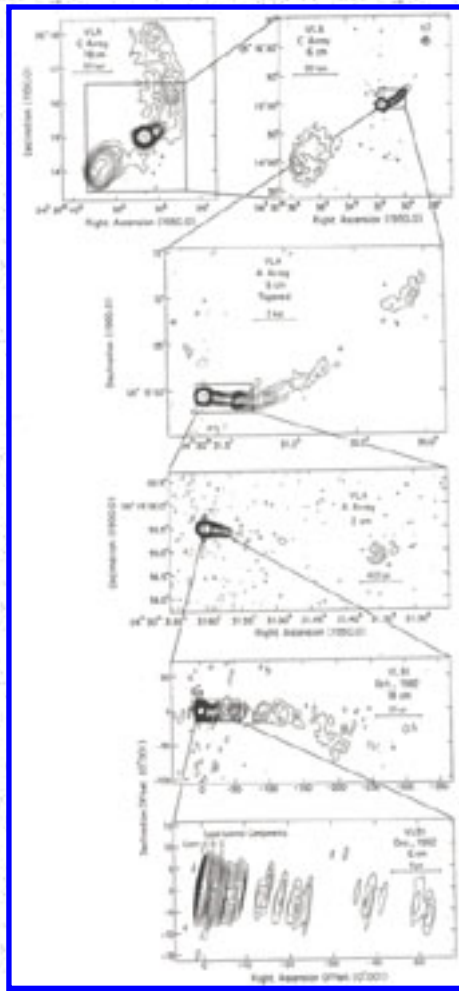


Figure 13.1. Contour maps of the radio galaxy [3C120](#), showing the structure over a wide range of angular scales (Walker et al. 1987).

13.1.1. Optical Counterparts

The optical identification of the discrete radio sources is important for two reasons. First, it is not possible from the radio measurements alone to determine the distance to a radio source. Only if there is an optical identification can the redshift and, from the Hubble law, the distance be determined. In this way it is then possible to calculate the absolute radio luminosity, linear size, and energy content from measurements of radio flux density and angular structure. Second, optical as well as X-ray and infra-red studies of the radio source counterparts may give some insight into the problem of the origin of the intense radio emission.

The coordinates of radio sources may be routinely measured with an accuracy better than one second of arc, generally permitting the unambiguous association with optical counterparts as faint as about 24th magnitude, which is reached with large reflectors and modern instrumentation. Nevertheless, due to the large amount of telescope time required for systematic studies of color and spectra, only for the strongest few hundred radio sources are the optical identifications reasonably complete (Spinrad et al. 1985). But

even for very weak radio sources, optical identifications are usually possible.

(a) Historical Background

The discrete sources of radio emission were first distinguished from the general background radiation as a result of their rapid amplitude variations at low frequencies, which were thought to be due to fluctuations in intrinsic intensity (Hey et al. 1946), but which we now recognize are due to scintillations in the earth's ionosphere. Considering that the dimensions of a variable source cannot greatly exceed the distance traveled by light during a characteristic variability time which is typically about one minute, it was generally thought that the discrete "variable" sources must be galactic stars; thus they were originally referred to as "radio stars."

When two of the strongest radio sources were identified by Bolton and Stanley (1949) with the nearby galaxies [M87](#) and [NGC 5128](#), it became clear that at least some of the discrete sources were extragalactic. Later the position of the powerful radio source [Cygnus A](#) was measured by Smith (1951) with sufficient precision to permit the identification by Baade and Minkowski (1954) with a relatively faint 15th-magnitude galaxy having redshift of 0.06. After this the extragalactic nature of the discrete sources was widely recognized, although the use of the term "radio stars" for extragalactic radio sources persisted for many years.

Other radio sources were identified with galaxies during the 1950s, but progress was slow because of the poor accuracy of the radio source positions. By the early 1960s, however, the increased use of interferometer systems led to position accuracies of the order of a few arcseconds, and many sources were identified with various galaxy types from inspection of the Palomar Sky Survey, which reaches a limiting magnitude about 20.

(b) Radio Galaxies

Galaxies which are identified with strong radio sources in the range of 10^{41} to 10^{46} ergs s^{-1} . are generally referred to as "radio galaxies." For the most part, radio galaxies are giant ellipticals with absolute visual magnitude about -21. ¹

Many intermediate-luminosity radio galaxies are found in rich clusters of galaxies. X-ray observations show that these clusters often contain a hot (10^8 K), relatively dense (10^{-3} particles per cm^{-3}) intracluster medium. Many of the radio in rich clusters show bends or distortions apparently associated with their interaction with this medium.

Many of the more powerful radio galaxies show bright optical emission lines in their nuclei whose strength appears to be correlated with the strength of the compact radio core (Heckman et al. 1983a). Radio galaxies with narrow emission lines in their spectrum are referred to as *narrow-line radio galaxies* (NLRG). Typical line widths are of the order of 1000 km s^{-1} . and include both forbidden lines of O, N,

S, and Fe as well as the Balmer lines of He. *Broad-line radio galaxies* (BLRG) have very broad H and He features, with velocities up to $25,000 \text{ km s}^{-1}$, and may also include narrow emission features as well.

Because of their bright emission lines, it is relatively easy to determine the redshift of many radio galaxies. Indeed, the most distant galaxy redshifts measured are those of radio galaxies. However, for redshifts much greater than unity, the optical K correction becomes very large. Due to the rapid decrease in the brightness of elliptical galaxies toward the blue part of the spectrum, highly redshifted radio galaxies appear very faint at visual wavelengths, but can often be observed in the near infrared.

(c) Quasars

In 1960, the relatively strong, small-diameter radio source [3C295](#) was identified with a 20th-magnitude galaxy having a redshift of 0.46, and was the most distant galaxy known at the time (Minkowski 1960). Continued efforts to identify distant galaxies concentrated on radio sources of small diameter and high surface brightness since these positions could be measured with high accuracy. In 1961, the small-diameter radio source [3C48](#) was identified with what appeared to be a 16th-magnitude *stellar* object. The subsequent discovery of night-to-night variations in the light intensity led to the reasonable conclusion that [3C48](#), unlike the other identified discrete radio sources, was indeed a true *radio star* in our galaxy. Soon, the optical counterparts of two other relatively strong small-diameter radio sources, [3C196](#) and [3C286](#), were also found to appear stellar, and it appeared that as many as twenty percent of all high-latitude radio sources were of this type.

Early efforts to interpret the emission line spectrum of the three known *radio stars* were unsuccessful although by 1962 some apparent progress was being made in associating many of the lines in the [3C48](#) spectrum with highly excited states of rare elements. However, lunar occultation measurements gave an accurate position of the strong compact radio source [3C273](#) (Hazard et al. 1963). Shortly afterward, Maarten Schmidt (1963) identified [3C273](#) with a 13th-magnitude stellar object, and he noted that the relatively simple spectrum could be interpreted as a redshifted ($z = 0.16$) Balmer series plus MgII.

A reinspection of the [3C48](#) spectrum indicated that if the bright line at 3832 \AA was identified with the MgII line at 3727 \AA in the rest frame, its redshift would be 0.37. Other lines in the [3C48](#) spectrum could then be identified with OII, NeIII, and NeIV. Additional spectra of other similar objects led to the identification of CIII, CIV, and finally Ly α , permitting much larger redshifts to be easily measured. The word *quasar* is now most often used to describe the entire class of highly redshifted *quasi-stellar objects* or QSOs.

Assuming that the measured redshifts are cosmological and the distance is given by the Hubble law with $H = 100 \text{ km s}^{-1} \text{ Mpc}^{-1}$, then the absolute visual magnitudes of quasars range from about -24 to -31. Thus, at optical wavelengths, quasars are up to a few hundred times brighter than the most luminous galaxies. Some relatively low redshift (nearby) quasars, which are strong radio sources, appear to be surrounded by a faint fuzz whose dimensions, color, and brightness are typical of giant elliptical

galaxies, thus supporting the idea that quasars are the extremely active nuclei of galaxies. Further down the optical (as well as radio) luminosity function are the Type II *Seyfert galaxies*, which have relatively bright nuclei with broad emission lines and absolute magnitudes of -20 to -23, the so-called *Markarian galaxies*, which were originally isolated on the basis of their large UV excess, on photographic plates, and the blazars and BL Lacs. The literature is not always consistent on nomenclature. We will use the term *AGN* to describe galaxies with prominent (active) nuclei and *quasar* for objects where the starlike component dominates although there may be a faint underlying galaxy.

The optical spectrum of quasars is clearly nonthermal with a typical spectral index $\alpha \sim -1$ [(flux density) \propto (frequency) $^\alpha$] which may continue to the near infrared ($2.2 \mu\text{m}$ as well as to X-ray wavelengths (see [Figure 13.2](#)). Because quasars have an ultra-violet excess compared with the spectra of galaxies, moderate redshifts will cause quasars to appear blue when measured by multi-color photometry or when the color is estimated from the "red" and "blue" plates of the Palomar Sky Survey. This property has proved useful in making optical identifications of radio sources with quasars, without taking individual spectra, but it is not infallible. For very large redshifts, the color may appear neutral or even "red" when compared with stars and galaxies, so the identification of high-redshift quasars depends on position coincidence alone and requires both radio and optical position accuracies of the order of an arcsecond.

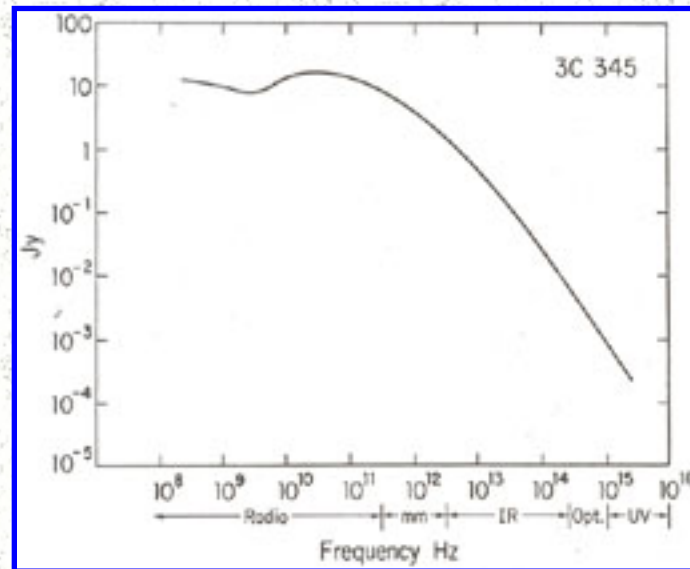


Figure 13.2. Spectrum of the quasar [3C345](#) from the radio through the ultraviolet part of the spectrum. Adopted from Bregman et al. (1986) with additional data from the radio literature.

Generally, quasar spectra show intense broad emission lines characteristic of a highly ionized gas with $T \sim 10^4$ K and $n_e \sim 10^8 \text{ cm}^{-3}$, line widths corresponding to velocities of $10,000 \text{ km s}^{-1}$ or more, and dimensions of the order of a parsec. The most commonly observed lines are those of Ly α (1216 \AA), CIII (1909 \AA), CIV (1549 \AA), MgII (2798 \AA), OIII (4363 \AA , 4959 \AA , 5007 \AA), and the hydrogen Balmer series.

In addition, there is a larger narrow-line emission region with densities $n_e < 10^7 \text{ cm}^{-3}$ producing forbidden emission lines. When examined with sufficient spectral resolution, most quasars also show numerous narrow absorption lines, but the unambiguous identification of quasar absorption lines is complicated by the presence of multiple redshift systems. In some cases the absorption redshift is close to the emission redshift, and these are believed to be intrinsic to the quasar or associated with its parent cluster. In other cases, the absorption redshift is much less than the emission redshift, and these are thought to originate in intervening clouds lying along the line of sight.

A relatively small number of compact radio sources are identified with optical objects which appear stellar, are highly variable at optical as well as at radio wavelengths, have a nonthermal optical spectrum, often very steep, with no emission or absorption lines, and are often strongly polarized at optical and radio wavelengths. These are frequently referred to as BL Lac objects (the prototype object is BL Lacerte), or *blazars*. The relation between quasars and blazars as well as the more classical elliptical radio galaxies has been the subject of much research and debate (see Wolfe 1978). A commonly discussed model considers the BL Lac objects as quasars with enhanced continuum emission which overrides the emission line spectrum. This picture is supported by the detection of faint emission lines in a few BL Lac objects at the time when the strength of the continuum emission is near a minimum.

Not all quasars are strong radio sources. Optical surveys using objective prisms to spot the characteristic bright emission line spectra of quasars or surveys of UV excess objects show that *radio-quiet* quasars are about ten times more numerous than the *radio-loud* quasars. Quasars with very broad emission lines, in particular, do not seem to be strong radio sources. High-sensitivity radio observations indicate that most optically selected quasars however are weak radio sources. The underlying or "host" galaxies of the radio-quiet quasars appear to be spirals, whereas the "hosts" of radio-loud quasars are probably elliptical galaxies. Quasars which are strong radio sources are usually strong X-ray sources.

¹ $H = 100 \text{ km s}^{-1} \text{ Mpc}^{-1}$. [Back](#).

13.1.2. Radio Source Properties

The radio-frequency spectra and polarization properties of radio galaxies and quasars are characteristic of synchrotron radiation from relativistic electrons having a power law distribution of electron energies with a Lorentz factor, $\gamma \sim 1000$ and a magnetic field strength $B \sim 10^{-5}$ gauss. The radio emission can be conveniently divided into two categories: the *extended* structure, which is *transparent*, and the *compact* structure, where the density of relativistic electrons is so great that the source becomes *opaque* to its own radiation. There is no simple relation between the structure or dimensions of the radio-emitting region and the dimensions of the associated optical galaxy or quasar, although there are clear statistical

differences. Most compact sources are identified with QSOs or with active galactic nuclei. However, less powerful compact sources are also found in normal-looking elliptical galaxies as well (see Ekers 1978, 1981 for a more complete discussion). The extended sources are typically associated with galaxies, but many are quasars with no visible optical extent. Most extended sources, particularly quasars, when examined with sufficient sensitivity and resolution, are found to contain a compact central radio component. The central components are particularly prominent in quasars (e.g., Owen and Puschell 1984). On the other hand, most compact sources, when examined with high sensitivity and dynamic range, exhibit weak extended radio structure. Because the compact sources are affected by self-absorption, their spectra are flat ([Section 13.1.3](#)). They are therefore most easily detected by radio surveys made at short wavelengths, whereas the steep-spectrum extended sources with their transparent spectra are characteristic of long-wavelength surveys. The terms *extended* (or lobe-dominated) source and *compact* (or core-dominated) source are often used to describe sources where the extended or compact structure, respectively, is most pronounced.

In the less powerful radio galaxies, the radio emission is often confined to the region of optical emission, or about 10 kpc, but in the more powerful radio galaxies, the radio emission comes from two well-separated regions hundreds of kiloparsecs across. In the giant radio galaxies, radio source dimensions larger than 3 Mpc have been observed. The compact features have dimensions typically ranging from 1 to 100 pc, although in a few nearby galaxies radio nuclei as small as 0.01 pc have been observed.

13.1.3. Radio Spectra

With the exception of the 21-cm line of neutral hydrogen, H₂O and OH found only in relatively nearby galaxies, there are no sharp features in the radio spectra of galaxies and quasars, and the observations are confined to measurements of the continuous spectra. Since individual radio telescopes generally operate only over a limited range of wavelengths, the determination of broadband spectra requires the combination of data obtained by many observers using many different types of telescopes. Because radio telescopes may differ widely in their characteristics, each antenna and radiometer system must be separately calibrated at every wavelength where observations are made. Generally, this is done by observing one or more sources whose intensity is known on an "absolute" scale. Standard sources calibrated with an absolute accuracy of a few percent are available over a wide range of wavelengths from short millimeter wavelengths to wavelengths of a few meters. The determination of relative intensities is much easier, at least at the shorter wavelengths where confusion from the galactic background is less of a problem.

Thousands of extragalactic sources have now been observed at decimeter and centimeter wavelengths, and for several hundred sources the spectra are complete over a range of wavelengths extending from a few millimeters to a few tens of meters (10 MHz to 100 GHz). In a few cases, the spectra extend to 1 mm (300 GHz), but measurements at short millimeter wavelengths are difficult due to the variable opacity of the atmosphere.

Radio spectra are usually displayed in the form of a logarithmic plot of flux density versus frequency

(see [Figure 13.3](#)). Sources with power law spectra are then represented by a straight line, with slope equal to the spectral index, α . Although the radio spectra of only a few sources follow such a simple power law accurately, a spectral index may be defined at any frequency as the derivative $d(\log S) / d(\log \nu)$ or by the measurement of flux density at two arbitrarily selected frequencies. The observed spectra of extended sources generally show negative curvature in the $\log S - \log \nu$ plane, that is, the spectrum becomes more steep at high frequency. Typically the region of curvature extends over a decade or so of frequency. At frequencies significantly removed from the maximum curvature, the spectrum can be represented by two well-defined power laws. Values of the spectral index of the extended radio features are in the range $-1.3 < \alpha < -0.5$, and over a wide range of frequencies show a strong concentration near -0.8 with a dispersion of only 0.15 . The steepest spectral index which is observed is about -2.0 and the flattest about -0.5 .

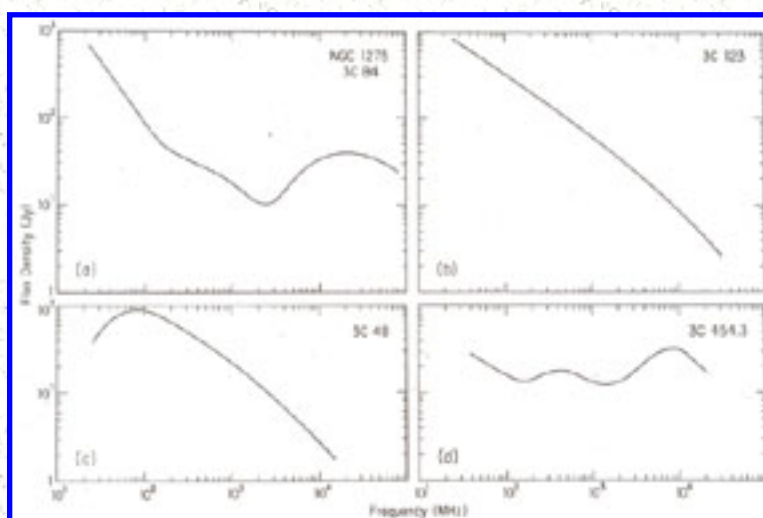


Figure 13.3. Typical radio-frequency spectra: (a) the radio galaxy [3C84](#), showing low-frequency power law component which comes from the large-scale structure, an intermediate-size feature which becomes opaque at a frequency of a few GHz, and the small nuclear source which is opaque below 20 GHz; (b) the radio galaxy [3C123](#) which is transparent throughout the observed range of frequency but has a spectrum which steepens at high frequencies; (c) the quasar [3C48](#) which has a self-absorption cutoff near 100 MHz and is transparent at higher frequencies; and (d) the quasar [3C454.3](#) which has multiple peaks due to the superposition of several features which become opaque at widely different frequencies.

Radio sources or components of sources with spectra flatter than -0.5 are nearly always very compact, and are coincident with a quasar or AGN. In these sources, the flat spectrum is thought to be the result of

self-absorption, rather than a flat electron energy distribution. In some sources, particularly quasars and BL Lac objects, the spectra remain opaque at least up to a few hundred GHz but steepen at the infrared and optical wavelengths to a spectral index of about -1 (e.g., Ennis et al. 1982, Landau et al. 1983, Bregman et al. 1986, Roellig et al. 1986). Some sources show a flattening toward the near UV, which is often referred to as the "3000 Å, bump." In general, only about ten percent of the radiation from quasars and AGNs is emitted at radio wavelengths, with most of the power being radiated at submillimeter wavelengths.

In the extended regions, where the relativistic plasma is transparent (optically thin) to its own radiation, and the observed spectral flux density is merely the sum of the radiation from the individual electrons and reflects the distribution, $N(E)$, of relativistic particle energy (see Chapter 1). In the case of a power law distribution of particle energies, $N(E) = KE^{-p}$, the radiation spectrum is a power law with $S \propto \nu^\alpha$, where the spectral index $\alpha \sim (1 - p) / 2$ (Equation 1.14). The characteristic spectral index $\alpha \sim -0.8$ frequently found in the extragalactic sources then corresponds to a value of $p \sim 2.6$, which is close to the index of primary cosmic-ray particles in the Galaxy.

Even if relativistic electrons are initially produced with a power law distribution, differential energy losses will alter the energy spectrum, so that it is steeper at higher energy. Relativistic electrons lose energy by synchrotron radiation and by the inverse Compton effect, which are both proportional to the square of the energy; by ordinary bremsstrahlung and adiabatic expansion, which are directly proportional to the energy; and by ionization, which is approximately proportional to the logarithm of the energy. Approximating the logarithmic term by a constant, the rate of energy loss may be written

$$\frac{dE}{dt} = aE^2 + bE = c. \quad (13.1)$$

If the electrons are being supplied to the source at a rate $N(E, t)$, then the equation of continuity describing the time dependence of the energy distribution $N(E, t)$ is

$$\frac{\partial N(E, t)}{\partial t} = \frac{\partial}{\partial E} \left(\frac{dE}{dt} \right) N(E, t) + N(E, t) \quad (13.2)$$

It is of interest to consider the case where synchrotron losses dominate ($b = c = 0$). Then from Equation (1.10), $a = -120 B^2$. If the initial particle distribution is a power law of the form $N(E) = K E^{-p}$ between E_1 and E_2 , and zero elsewhere, and if there is no continual injection or acceleration, then the energy distribution will remain a power law with the same slope, but with an amplitude which decreases with time according to

$$N(E, t) = \frac{KE^{-p}}{(1 - 120B^2Et)^2} \quad \text{for } E_1' < E < E_2' \quad (13.3)$$

where $E' = E / (1 + 120 B^2 E t)$. Thus, even with an initial energy distribution extending to unlimited energy, after a time t years, there will be an upper energy cutoff at

$$E_c = \frac{1}{120 B^2 t} \text{ GeV.}$$

From Equation (1.8) there is a corresponding cutoff in the synchrotron radiation spectrum at a frequency $\nu_b \sim B^{-3} t \text{ (yr)}^{-2} \text{ GHz}$.

If the distribution of electron pitch angles is random, the cutoff frequency for each pitch angle differs. At low frequencies where energy losses are not important, the spectral index, α , remains equal to its initial value $\alpha_0 = (1 - p) / 2$. If the pitch angle distribution is conserved, then for $\nu \gg \nu_b$, $\alpha = 4/3 (\alpha_0 - 1)$ (Kardashev 1962). If, on the other hand, the pitch angle distribution is continuously made random, for example, by irregularities in the magnetic field, then all the electrons see the same effective magnetic field and the spectrum will show the same sharp cutoff which is observed with a single pitch angle. No such cutoff is observed, even for those sources whose spectra are determined out to 100 GHz or more.

If relativistic electrons are continuously injected with $Q(E) = K E^{-p_0}$, then for $\nu \ll \nu_b$ the spectral index again remains constant with $\alpha = \alpha_0$ [$\alpha_0 = (1 - p_0) / 2$]. But for $\nu \gg \nu_b$ where the rate of energy loss is balanced by the injection of new particles, the equilibrium solution of Equation (13.2) with $(\partial N / \partial t) = 0$ gives $\alpha = (\alpha_0 - 1/2)$.

Observations over the frequency range 10 MHz to 100 GHz show curvature of the form expected from synchrotron radiation losses, with $\nu_b \sim 1 \text{ GHz}$. Typically, $\Delta \alpha \sim 1/2$, as expected if relativistic electrons are continually supplied. If a few sources $\Delta \alpha \sim 1$, suggesting that in these sources particle acceleration may have ceased.

Quantitative analysis is difficult, since the spectra may vary across the source, particularly if the magnetic field is not constant. Generally, the hot spots and jets appear to have flatter spectra than the more extended diffuse components, apparently reflecting their younger ages and correspondingly smaller synchrotron radiation losses. The very diffuse components associated with clusters have the steepest observed radio spectra with indices generally steeper than -1.

13.1.4. Energy Considerations

The problem of the origin and evolution of extragalactic radio sources is a formidable one; in particular, the source of energy needed to account for the large power output and the manner in which this energy is converted to relativistic particles and magnetic flux is a subject of considerable debate. Assuming only that synchrotron radiation from ultra-relativistic electrons is responsible for the observed radiation, the necessary energy requirements were shown by Burbidge (1958) to be as much as 10^{60} ergs or more.

Following Burbidge, if the relativistic particles have a power law distribution with an index p between E_1 and E_2 , then for $p \neq 2$, the energy contained in relativistic electrons is

$$E_e = \int_{E_1}^{E_2} EN(E)dE = \frac{K}{(2-p)} [E_2^{(2-p)} - E_1^{(2-p)}]. \quad (13.4)$$

The constant K can be evaluated if the distance to the source is known. The total luminosity, L , is given by integrating Equation (1.10), or

$$\begin{aligned} L &= \int_{E_1}^{E_2} N(E) \frac{dE}{dt} dE = \int_{E_1}^{E_2} 120B^2 E^{(2-p)} dE \\ &= 120 \frac{KB^2}{(3-p)} [E_2^{(3-p)} - E_1^{(3-p)}]. \end{aligned} \quad (13.5)$$

For $p = 2.5$, and $q_0 = +1$, $L \sim 10^{44} z^2 S$, where S is the flux density at 1 GHz. ²

Eliminating K between Equations (13.4) and (13.5) we have

$$E_e = \frac{L}{120} \left(\frac{3-p}{2-p} \right) \left(\frac{E_2^{(2-p)} - E_1^{(2-p)}}{E_2^{(3-p)} - E_1^{(3-p)}} \right) \text{ ergs.} \quad (13.6)$$

Using Equation (1.8) to relate E_2 and E_1 to the cutoff frequency and grouping all the constant terms together,

$$E_e = C_e(p) LB^{-3/2}. \quad (13.7)$$

The total luminosity L of the source may be estimated by integrating the observed spectrum between 10 MHz and 100 GHz. The magnetic energy is obtained from

$$E_B = \int \frac{B^2}{8\pi} dV = C_B B^2 V. \quad (13.8)$$

The total energy in fields and particles ($E_c = E_e + E_B$) is minimized when $dE / dB = 0$ or when

$$B_{\min} = \left(\frac{3 C_e L}{4 C_B V} \right)^{2/7} \sim 1.5 \times 10^{-4} \theta^{9/7} z^{-2/7} S^{2/7} \text{ gauss.} \quad (13.9)$$

The value of B estimated in this way must be treated with caution. It depends almost entirely on the angular size, θ , and is relatively insensitive to the flux density, distance, or spectral index.

From Equations (13.7), (13.8), and (13.9), if θ is expressed in arcseconds, then

$$(E_e)_{\min} \sim \frac{4}{3} (E_B)_{\min} \sim 10^{59} \theta^{9/7} z^{17/7} S^{4/7} \text{ ergs} \quad (13.10)$$

and depends only weakly on p . Thus, the minimum energy is given when the energy is nearly equally distributed between relativistic particles and the magnetic field, and this is usually referred to as the *minimum energy* or *equipartition* case.

Typically, the total energy contained in the extended sources is estimated to be in the range of 10^{57} to 10^{61} ergs and the magnetic field between 10^{-6} and 10^{-4} gauss. Under these near equilibrium conditions ($E_e \sim E_B$), the total energy depends to a large extent on the size of the source ($E \propto r^{9/7}$). Thus the larger sources with low surface brightness and low luminosity, such as [Centaurus A](#), are calculated to contain almost as much energy as the smaller but much more powerful high-surface-brightness objects such as [Cygnus A](#) or [3C295](#). However, high-resolution observations indicate that in many sources the observed radio emission comes from only a small fraction, Φ , of the projected volume. The minimum total energy calculated from Equations (13.9) and (13.10) is then multiplied by a factor of $\Phi^{3/7}$, and the corresponding magnetic field is increased by the factor $\Phi^{-2/7}$. It is by no means clear that minimum energy, or equivalently equipartition, conditions hold in extragalactic radio sources. Moreover, the value of the fill-in-factor Φ , is very uncertain, and calculation of energy content or magnetic field strength based on minimum energy or equipartition arguments must be treated with caution.

For some years it was widely thought that the relativistic electrons were secondary particles produced as the result of collisions between high-energy protons. If the ratio of the number of protons to electrons is k , then the minimum total energy is increased by a factor of $(1 + k)^{4/7}$ and the magnetic field by $(1 + k)^{2/7}$. Some estimates of the value of k were as high as 100, with a corresponding increase in energy requirements by about an order of magnitude. Elimination of the factor k and inclusion of the fill-in factor Φ , can easily reduce the minimum-energy estimates by two or more orders of magnitude.

A more direct, although not necessarily more accurate, method of determining the magnetic field in extended extragalactic radio sources is based on the scattering of the microwave background radiation by the relativistic plasma. The ratio between the synchrotron radio flux and Compton scattered X-ray flux depends on the magnetic field strength and is given approximately by (Miley 1980)

$$B \sim \{6.6 \times 10^{-40} (4800)^\alpha (1+z)^{3-\alpha} [S(\nu)/S(x)] \nu^{-\alpha} E(x)^{-\alpha}\}^{1/(1-\alpha)} \text{ gauss} \quad (13.11)$$

where $S(\nu)$ is the radio flux density at frequency ν and $S(x)$ is the X-ray flux density at energy $E(x)$. Values of B estimated from Equations (13.9) and (13.11) are in the range of 10^{-6} to 10^{-4} gauss, so that the energy content appears to be close to the minimum requirement. But estimates of B from Equation (13.11) are subject to error if the thermal X-ray flux is not negligible compared with the Compton scattered X-ray flux.

In a 10^{-4} -gauss field, electrons radiating at $\nu > 1$ GHz are expected to decay in about 10^6 years (Equation 1.8). Thus, the absence of any observed spectral cutoff even at $\nu \gg 10$ GHz suggests continued acceleration of relativistic particles. Even more restrictive limits are imposed by the observation of both radio and optical ($\nu \sim 10^{14}$ Hz) synchrotron emission from the [M87](#) jet at least 10 kpc away from the nucleus (Biretta et al. 1983a).

Because an adiabatically expanding cloud of relativistic particles loses energy as R^{-2p} (e.g. Kellermann and Pauliny-Toth 1968), it has been argued that if the observed relativistic electron clouds had expanded adiabatically from a much smaller region, the initial energy requirements would be prohibitively large. Although a variety of models have been discussed which allow some of the kinetic energy of expansion to be converted into relativistic particle energy, the adiabatic loss problem has been a prime motivation for models which consider the primary energy source to be in a compact region at the quasar or AGN with the energy being transported from this "central engine" to the outer lobes by a relativistic *beam*. ([Section 13.4.1](#)). However, it has also been pointed out by Bicknell (1986) and others that if the source has expanded to some final size and another burst of particles occurs, without significantly expanding the source, then no further adiabatic losses occur.

² Numerical expressions given in this chapter are evaluated for $H = 100 \text{ km s}^{-1} \text{ Mpc}^{-1}$, $q_0 = 1$, and $p = 2.5$ ($\alpha = 0.75$). More general formulations for other values of γ and more complex geometries are given in Moffet (1975), Jones et al. (1974a,b), and Marscher (1983). [Back](#).

13.2. LOW-LUMINOSITY SOURCES

The powerful radio galaxies and quasars have been recognized largely as a result of the optical identification of radio sources that have been catalogued in various radio surveys. By contrast, sources at the low end of the radio luminosity function are observed primarily by measuring the radio emission from known optical objects. The most extensive surveys are those of Sadler (1984), Kotanyi (1980), Hummel (1980), and Dressel and Condon (1978). These so-called "normal galaxies" typically have a radio luminosity between 10^{36} and $10^{39} \text{ erg s}^{-1}$. They are primarily ellipticals, but some spirals are also detected as weak radio sources (e.g., Ekers 1978, 1981, Sadler 1984, Preuss 1987).

The observed radio emission may come from an extended component comparable in size to the optical image or from a bright compact nucleus. Although the luminosities of the weak radio nuclei are some million times less than those found in radio galaxies and quasars, the surface brightness, magnetic field strength, structure, and time scale of observed intensity variations are all comparable to those of their more luminous counterparts discussed in [Section 13.3](#).

13.2.1. Spiral, Seyfert, and Irregular Galaxies

For normal spiral galaxies, much of the radio emission comes primarily from the disk. In a few nearby spirals where the distribution of radio emission can be mapped, the spiral structure is clearly evident. This diffuse component of the nonthermal emission appears to be unrelated to that of the much more luminous radio galaxies and quasars but rather to the optical luminosity and morphology of the galaxy. High-resolution observations indicate that the characteristic size of radio nuclei of spirals is about 100 pc, but significant emission sometimes comes from a region less than a parsec across (Dressel and Condon 1978, Hummel 1980, van der Hulst 1981, Heckman et al. 1983a).

These latter sources are probably related to the powerful compact sources found in AGNs and quasars. The discovery of flat-spectrum, compact, variable sources in the nuclei of [M81](#) and [M104](#) (de Bruyn et al. 1976) gave the first evidence of activity in the nuclei of normal spirals of the -type characteristic of quasars and AGNs. High-resolution VLBI observations of [M81](#) show that the radio nucleus is only about 0.01 pc in extent. Based largely on the presence of narrow emission lines in the optical spectrum, [M81](#) is sometimes classified as a Seyfert galaxy. But most Seyfert galaxies are not strong radio sources, although a few, such as [NGC 1068](#), have prominent radio cores and jets which have been, extensively studied (e.g., Wilson 1982). Often the cores of Seyfert galaxies show a low-frequency spectral turnover due to free-free absorption by ionized gas in the emission-line region, with emission measures in the range of 10^4 to 10^6 cm². Meurs and Wilson (1984) discuss the radio emission from Seyfert galaxies and their relation to other radio sources.

A small fraction of spiral and irregular galaxies show enhanced radio emission which is closely correlated with the 10 - μ m infrared flux density and apparently corresponds to regions where there are bursts of star formation (e.g., Condon 1982). At one time the dramatic visual image of [M82](#), particularly in H α , was interpreted as evidence of explosive activity characteristic of the powerful radio galaxies. More recent work, however, has shown that the radio emission from [M82](#) comes from a number of small (less than a few parsecs) discrete components probably related to supernovae events or to regions of intense star formation with intrinsic luminosities as much as 100 times that of Cas A. The strongest of these is known to be variable and is only a few hundred AU in size (Kronberg et al. 1981).

Observations by Stocke (1978) indicate enhanced radio emission from interacting pairs of galaxies, although, curiously, the excess emission comes primarily from a compact core, and not from the disk (e.g., Hummel 1980).

13.2.2. Elliptical Galaxies

Weak compact radio sources are frequently found in the nuclei of elliptical galaxies, particularly those with bright emission-line nuclei and those in which 21-cm observations show the presence of significant amounts of HI. These are high-surface-brightness compact sources which are frequently variable on time scales of months to years. When examined with high angular resolution, the weak radio nuclei typically show the same characteristic asymmetric core jet structure which is observed in the nuclei of the more powerful radio galaxies and quasars (e.g., Jones et al. 1984, Wrobel et al. 1985). Often there is also large-scale structure on a scale of a kiloparsec to a few hundred kiloparsecs comparable to that found in the powerful radio sources (e.g., Wrobel and Heeschen 1984).

13.3. COMPACT SOURCES

13.3.1. Self-Absorption

When the apparent source brightness temperature approaches the equivalent kinetic temperature of the relativistic electrons, synchrotron self-absorption becomes important, and part of the radiation is absorbed by the relativistic electrons along the propagation path. Below the self-absorption cutoff frequency, the spectrum is just that of a blackbody with an equivalent temperature $T_k = E / k$.

From Equation (1.8), $E \propto \nu^{1/2}$, so in an opaque synchrotron source the flux density $S \propto \nu^{2.5}$, rather than the ν^2 law found in thermal sources. In other words, an opaque synchrotron source may be thought of as a body whose equivalent temperature depends on the square root of the frequency. Self-absorption occurs below a frequency ν_c where the kinetic temperature

$$T_k = \frac{E}{k} \sim 8 \times 10^3 B^{1/2} \nu^{1/2} k^{-1} \text{ K},$$

is equal to the brightness temperature

$$T_B = S \theta^{-2} c^2 (2k)^{-1} \nu^{-2} \text{ K}.$$

Assuming uniform source parameters, the magnetic field can then be estimated from observation of ν_c and surface brightness from

$$\nu_c \sim f(p) B^{1/5} \theta^{2/5} S_m^{-4/5} (1+z)^{1/5} \delta^{-1/5} \text{ GHz} \quad (13.12)$$

where S_m is the maximum flux density in janskys, ν_c the cutoff frequency in GHz, and θ the angular size in milliarcseconds. The quantity δ is a correction for the relativistic Doppler shift if the source is

moving with high velocity (see [Section 13.3.7](#)). If $\nu \ll c$, $\delta \sim 1$. The function $f(p)$ only weakly depends on geometry and the value of p , and is about 8 for $p \sim 2.5$. Variations in opacity throughout the source give an overall spectrum that can be considered as the superposition of many simple regions described by Equation (13.2) and can give rise to the so-called *flat* or undulating spectra typically observed in compact radio sources (e.g., Condon and Dressel 1978).

The magnetic field in a compact radio source can be determined directly from the observables θ , S_m , and ν_c by Equation (13.12). The magnetic energy, E_B , can be estimated from Equation (13.8) to be

$$E_B \sim 2.5 \times 10^{48} S_m^{-4} \theta^{11} \nu_c^{10} (1+z)^{-2} \delta^2 z^3 \text{ ergs.} \quad (13.13)$$

Similarly, from Equation (13.6), the energy in relativistic electrons is given approximately by

$$E_e \sim 3.1 \times 10^{62} \left(\frac{S_{\max}}{\theta^2} \right)^{5.5} \nu_c^{-10.5} z^2 \text{ ergs.} \quad (13.14)$$

Synchrotron radiation losses lead to a characteristic half-life at a frequency ν_m of

$$t \sim B^{-3/2} \nu_m^{-1/2} \sim 10^7 S^3 \theta^6 \nu_c^{-8} \delta^{3/2} (1+z)^{3/2} \text{ years.} \quad (13.15)$$

In practice, the use of Equations (13.13) and (13.14) to derive the magnetic and particle energy is difficult due to the strong dependence on angular size and cutoff frequency. However, in almost every case where measurements exist, the particle energy appears to greatly exceed the magnetic energy. But note the dependence on θ and ν_c to about the tenth power; so small changes in the geometry may lead to other conclusions. The ratio of E_e / E_B may also be reduced considerably with even modest values of δ . See [Section 13.3.6](#).

13.3.2. Inverse Compton Radiation

In very compact sources, in which the radiation energy density is comparable to the magnetic energy density, inverse Compton scattering will cause additional electron energy losses. For a homogeneous isotropic source

$$\frac{L_c}{L_s} = \frac{U_{\text{rad}}}{U_B} = \frac{24L}{d^2 B^2 c} \quad (13.16)$$

where L_c is the power radiated by inverse Compton scattering, $L_s \sim 4\pi R^2 S_m \nu_c$ is the radio power radiated by synchrotron emission, $U_{\text{rad}} = 3L / 4 d^2 c$ is the energy density of the radiation field, $U_B =$

$B^2 / 8\pi$ is the energy density of the magnetic field, R is the distance to the source, θ the angular size, and $d = R\theta$ is the source diameter. Then, from Equation (13.16), recognizing that $S_m / \theta^2 \nu^2$ is proportional to the peak brightness temperature, T_m , and including the effect of second-order scattering, we have

$$L_c / L_s \sim \frac{1}{2} \left(\frac{T_m}{10^{12}} \right)^5 \nu_m \left[1 + \frac{1}{2} \left(\frac{T_m}{10^{12}} \right)^5 \right] \quad (13.17)$$

where ν_m is the spectral upper cutoff frequency. Taking $\nu_m \sim 100$ GHz, when $T < 10^{11}$, $L_c / L_s \ll 1$, inverse Compton scattering is not important. But when $T > 10^{12}$ K, the second-order term becomes important, $L_c / L_s \sim (T_m / 10^{12})^{10}$, and inverse Compton losses become catastrophic. The exact value of the peak brightness temperature which corresponds to the case where $L_c \sim L_s$ is somewhat dependent on the specific geometry, the value of p , and the spectral cutoff frequency, ν_m , but the strong dependence of L_c / L_s on T_m means that the maximum brightness temperature, T_m , cannot significantly exceed 10^{12} K, independent of wavelength. This places a lower limit to the angular size of

$$\theta \gtrsim 10^{-3} S_m^{1/2} \nu_c^{-1} \text{ milliarcseconds.} \quad (13.18)$$

Observations show that the peak brightness temperature of compact radio sources measured by VLBI is almost always in the range of 10^{11} to 10^{12} K. Thus, the angular size of an opaque source can be estimated from the peak flux density, S_m , and the self-absorption cutoff frequency, ν_c to give

$$\theta \sim S_m^{1/2} \nu_c^{-1} (\text{GHz}) \text{ milliarcseconds.} \quad (13.19)$$

The observed angular size is generally in good agreement with that expected from Equation (13.19) and the measured peak flux density and cutoff frequency, and there is no evidence that the peak brightness temperature ever exceeds 10^{12} K. This is strong evidence that the compact radio sources indeed radiate by the synchrotron process, and that the radio emission is limited by inverse Compton cooling.

The inverse Compton scattered flux density, S_c , at an energy E is given by Marscher (1983) as

$$S_c \sim \ln(\nu / \nu_m) \theta^{-2(p+3)} \nu_m^{-1/2(3p+7)} S_m^{(p+3)} E^{-1/2(p+1)} (1+z)^{(p+3)} \delta^{-(p+3)} \mu\text{Jy.} \quad (13.20)$$

where ν_m is the upper cutoff frequency of the synchrotron radiation spectrum.

Near the $E = 1$ keV band of the Einstein Observatory, this becomes (Biermann and Zensus 1984)

$$S_c \sim T_B^{p+2} S_V^{(p+1)/2} (1+z)^{p+3} \delta^{-(p+3)} \mu\text{Jy} \quad (13.21)$$

where the effective brightness temperature, T_B , is approximately $\nu^2 \theta^2 S / 1.22$ when T_B is expressed in units of 10^{12} K.

Observations at millimeter wavelengths, where the effect of self-absorption is small, do indeed show a correlation between measured radio and X-ray flux density in the sense expected if the X-ray emission is due to inverse Compton scattering from the radio photons (Owen et al. 1981).

13.3.3. Polarization

As described in [Section 13.1](#), in a uniform magnetic field with a power law distribution of electron energies having an index p , the linear polarization, $P_t(p)$, of a transparent source is perpendicular to the direction of the magnetic field and is given by

$$P_t(p) = \frac{3p + 3}{3p + 7} \quad (13.22)$$

which is of the order of 70% for typical values of p .

In the opaque portion of the spectrum, the polarization is parallel to the magnetic field and is given by

$$P_o(p) = \frac{3}{6p + 13} \quad (13.23)$$

so that P_o is typically only about 10% or less. Observations of integrated polarization are typically much less than that predicted for a uniform field by at least an order of magnitude, presumably due to the random orientation of the magnetic fields.

The observed polarization position angle is modified by Faraday rotation (Section 1.2.2). Although most of the rotation occurs primarily within our galaxy (Section 1.5.4), some is internal to the sources. In a few cases, the internal rotation measure is surprisingly large with measured values up to several thousand radians per meter².

There appears to be no evidence for internal Faraday rotation in the compact radio sources. This places strict limits on the number of thermal electrons that can coexist with the relativistic electron cloud (Wardle 1977, Jones and O'Dell 1977). Indeed, the absence of Faraday rotation requires that the number of relativistic electrons must greatly exceed the number of cold (thermal) electrons, or that there are both electrons and positrons. Moreover, the number of low-energy relativistic electrons must be much less than the number expected from a power law extrapolation of the high-energy population. This has

important implications for possible acceleration mechanisms, and would appear to exclude most stochastic processes.

The synchrotron radiation from a single electron is elliptically polarized and has a large circular component which is mostly canceled if the pitch angle distribution is isotropic. However, there is still a small net circular polarization, since there are more electrons in the solid angle defined by $\theta + d\theta$ than in the one defined by $\theta - d\theta$. This effect is particularly important if the cone of radiation of a single electron ($\theta \sim mc^2 / E$) is large, which will occur at very low frequencies or in regions of high magnetic field strength (small values of electron energy).

In a uniform magnetic field of B gauss, and isotropic distribution of electron pitch angles, the integrated circular polarization is $P_c \sim (3B / \nu)^{1/2}$ at a frequency ν (Sciama and Rees 1967). In a few sources the degree of circular polarization has been measured to be $\sim 0.01\%$ to 0.1% near 1 GHz. This corresponds to magnetic fields of $\sim 3 \times 10^{-5 \pm 1}$ gauss - in good apparent agreement with the values derived from the synchrotron self-absorption cutoff frequency and the angular size.

13.3.4. Structure

Recent improvements in image formation techniques using interferometer baselines of thousands of kilometers (VLBI) now permit images of compact radio sources to be made with resolutions better than one milliarcsecond. Detailed radio pictures of quasars and galactic nuclei are now possible on a scale which is typically of the order of a few parsecs even for the most distant objects. For nearby galaxies, it is considerably less.

When mapped in detail (see [Figure 13.4](#)), the compact sources show a variety of structural forms. The great majority have asymmetric structure containing a bright region plus an elongated feature which resembles the jets seen on larger scales. These jetlike features often break up into a number of distinct components with different surface brightness and self-absorption cutoff frequency.

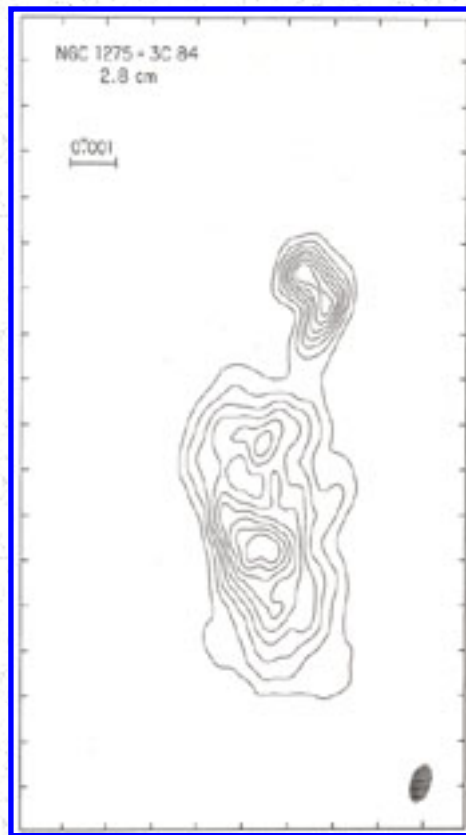


Figure 13.4. Milliarcsecond structure of the radio galaxy [NGC 1275 \(3C84\)](#) measured by VLBI (Romney et al. 1984).

Equation (13.19) indicates that for a wide range of magnetic field strength, there is a characteristic size of compact radio sources which varies with the wavelength of observation. Although there may be a big spread of the opacity in each source, individual components are most readily observed at the wavelength where the flux density is near a maximum (opacity of the order of unity). Thus, when observed over a range of frequency, individual sources show structural features ranging from a few tenths of a milliarcsecond or less at short centimeter wavelengths to a few hundredths of an arcsecond or more at longer wavelengths. The integrated spectrum, which is the sum of many peaked self-absorbed components, often is remarkably flat and shows an average spectral index near zero. Comparison of component sizes and self-absorption cutoff frequency, ν_c , indicate magnetic field strengths in the range of 10^{-4} to 10^{-2} gauss (Equation 13.12), but the observational uncertainties are very large as the derived value of B depends on ν_c^5 and θ^2 .

When there is an extended jet (see [Section 13.4.1](#)), it always lies on the same side of the core as the compact jet. Characteristically, the compact features are curved through an angle of a few tens of degrees, although in some cases the curvature extends through more than ninety degrees. The curvature is most pronounced near the inner region of the jet as it emerges from the core. The outer parts of the compact jets are usually aligned with the larger-scale jets, which are up to hundreds of kiloparsecs away. The alignment of these features over size scales ranging up to a factor of 100,000 means that the large

jets are focused and collimated within a region less than a parsec across. This remarkable feature of extragalactic radio sources implies a unique axis which extends from a parsec to a few hundred kiloparsecs, and a current activity with a "memory" extending back at least 10^5 to 10^6 years.

Some sources have a well-defined self-absorption cutoff frequency, usually at a relatively low frequency of a few hundred MHz. Above this frequency, the spectra are characteristic of transparent sources. VLBI observations often show that these sources have complex angular structure with overall angular sizes about 0.1 arcsecond, corresponding to the relatively low self-absorption cutoff frequency. Other sources of this type which are generally referred to as *Steep-Spectrum Compact Sources* have two similar well-separated components with no evidence for any jet structure.

There appears to be no obvious difference in structure between the compact components in sources with weak extended structure and the weak compact sources which are located near the center of strong double-component extended sources.

13.3.5. Variability

Nearly all compact radio sources, when observed over a sufficient period of time and with sufficient precision, show variability on time scales ranging from a few days to a few years and with fractional flux density changes ranging from a few percent to about 100 percent. The most rapid variations occur in BL Lac objects. In general, the observed variations may be described as outbursts which are strongest at the highest frequencies and propagate toward lower frequencies with reduced amplitude ([Figure 13.5](#)) (e.g., Dent et al. 1974, Dent and Kapitsky 1976, Altschuler and Wardle 1977, Andrew et al. 1978, Fanti et al. 1981, 1983, Epstein et al. 1982, Aller et al. 1985). However, the variations which are observed at frequencies less than 1 GHz or so for the most part appear unrelated to those observed at centimeter wavelengths and, as discussed below, are probably due to a different phenomenon.

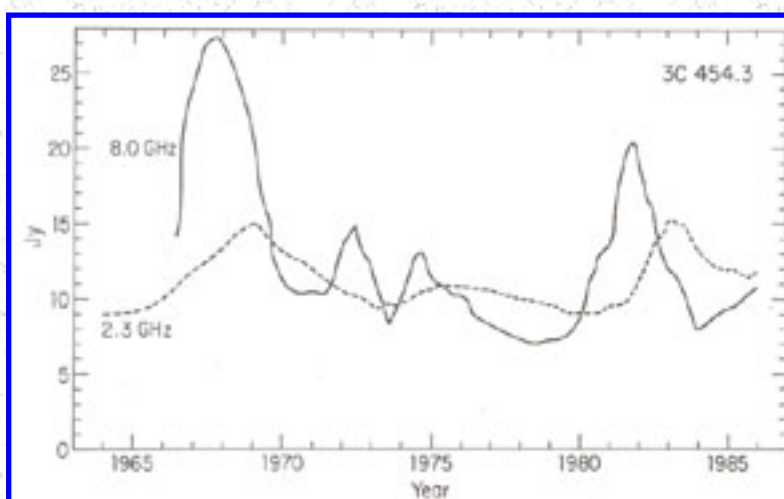


Figure 13.5. Variations in the flux density of the quasar [3C454.3](#) observed over a wide range of wavelengths. [Data taken from Allen et al. (1985); Altschuler and Wardle (1977), with permission from the Royal Astronomical Society; and Pauliny-Toth et al. (1987). Reprinted by permission from Nature, Vol. 328, No. 6133, pp 778. Copyright(c) 1987, Macmillan Magazines Ltd.]

The observation of variations in polarization is difficult since the degree of linear polarization is typically only a few percent, and the time scale for significant changes appears to be more rapid than for variations in total flux density (e.g., Allen et al. 1985). There appears to be no clear pattern to the variations in observed polarization. In some sources, there is a preferred orientation and the position angle remains constant throughout several flux density outbursts; in others, the direction may change even in the absence of obvious changes in total intensity.

Except for the most rapid variations, it is convenient to discuss the observed variations in terms of an expanding cloud of relativistic particles which is initially opaque out to short wavelengths but which becomes optically thin at successively longer wavelengths. In its simplest form, the model assumes that the relativistic particles are homogeneously distributed, that they initially have a power law spectrum, that they are produced in a very short time, in a small space, that the subsequent expansion occurs in three dimensions at a constant velocity, and that during the expansion the magnetic flux is conserved. Thus $\theta_2 / \theta_1 = t_2 / t_1$, and $B_2 / B_1 = (\theta_1 / \theta_2)^2 = (t_1 / t_2)^2$, where θ is the angular size, t the elapsed time since the outburst, B the magnetic field, and the subscripts 1 and 2 refer to measurements made at epochs t_1 and t_2 . The discussion below follows that of Kellermann and Pauliny-Toth (1968) and van der Laan (1966), and is based on ideas first described by Shklovsky (1965).

The observed flux density as a function of frequency, ν , and time, t , is shown in [Figure 13.6](#) and is described by

$$\frac{S(\nu, t)}{S_{m_1}} = \left(\frac{\nu}{\nu_{m_1}} \right)^{5/2} \left(\frac{t}{t_1} \right)^3 \times \left\{ \frac{\exp[-\tau(\nu/\nu_{m_1})^{-(p+4)/2}(t/t_1)^{-(2p+3)}]}{1 - \exp(-\tau)} \right\} \quad (13.24)$$

where S_{m_1} is the maximum flux reached at frequency ν_{m_1} at time t_1 .

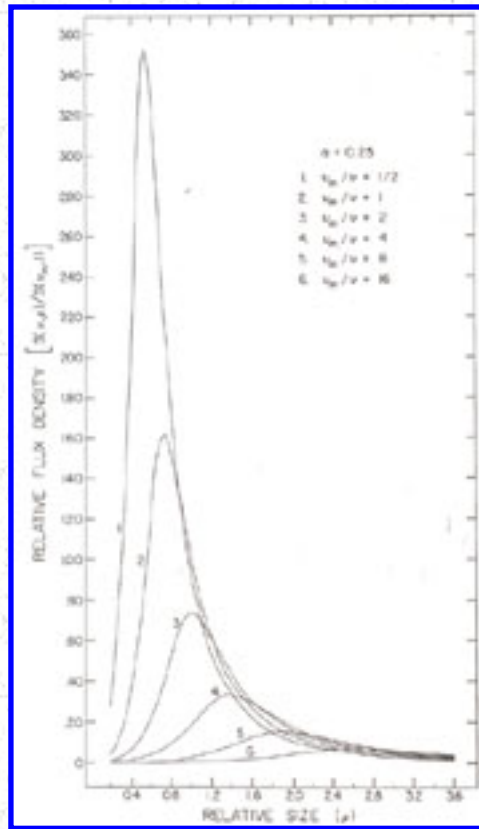


Figure 13.6. Variation in flux density and frequency for adiabatically expanding homogeneous source (van der Laan, 1966. Reprinted by permission from Nature, Vol. 211, No. 5054, pp. 1131. Copyright(c) 1966. Macmillan Magazines Ltd.)

If the optical depth, τ , is taken as the value at the frequency, ν_m at which the flux density is a maximum, then it is given by the solution of

$$e^{\tau\nu} - \left(\frac{p+4}{5}\right)\tau\nu - 1 = 0. \quad (13.25)$$

The maximum flux density at a given frequency as a function of time occurs at a different optical depth, τ_t , given by the solution of

$$e^{\tau\nu} - \left(\frac{2p+3}{3}\right)\tau\nu - 1 = 0. \quad (13.26)$$

In the region of the spectrum where the source is opaque ($\tau \gg 1$), the flux density increases with time as $S_2/S_1 = (t_2/t_1)^3$. Where it is transparent ($\tau \ll 1$), the flux density decreases as $S_2/S_1 = (t_2/t_1)^{-2\gamma}$.

The frequency, ν_m , at which the intensity is a maximum is given by

$$\nu_{m_2}/\nu_{m_1} = (t_2/t_1)^{-(4p+6)/(p+4)} \quad (13.27)$$

and the maximum flux density, S_m , at that frequency is given by

$$S_{m_2}/S_{m_1} = (\nu_{m_2}/\nu_{m_1})^{(7p+3)/(4p+6)} \quad (13.28)$$

Quantitative comparison with observations is difficult since most sources have multiple outbursts which overlap in frequency and time (e.g., [Figure 13.6](#)). Moreover, while a homogeneous, isotropic, flux-conserving model with constant expansion velocity is mathematically simple, more realistic models must consider nonconstant expansion rates, nonconservation of magnetic flux, changes in the electron energy index, p , the finite acceleration time for the relativistic particles, the inhomogeneous distribution of relativistic plasma, and the initial finite dimensions. In those few cases where individual outbursts may be isolated, the observed variations qualitatively conform to the simple model, with S_m , t_m , and ν_m described by Equations (13.27) and (13.28) with $1 \lesssim p < 1.5$. In general, however, the observed variations at the lower frequencies are larger than expected from an adiabatically expanding source, and it appears to be necessary to include the effect of continued particle injection or acceleration (e.g., Peterson and Dent 1973). Models which consider expansion along only one dimension, as expected from a jet, may also be more realistic than a spherical expansion.

Because the source dimensions are initially finite, the initial spectrum is always transparent at frequencies higher than some critical frequency, ν_0 . Above this frequency, the flux density variations occur simultaneously at all frequencies and reflect only the rate of relativistic particle production or decay due to synchrotron and inverse Compton radiation losses. Characteristically, ν_0 is in the range of 10 to 30 GHz. From Equation (13.18) this gives an initial size of $\sim 10^{-3}$ arcseconds for $B \sim 1$ gauss, corresponding to linear sizes of a few parsecs at $z \sim 1$. In those sources where good data exist in the spectral region $\nu > \nu_0$, the observed variations occur with roughly equal amplitude at all frequencies, indicating an initial spectral index $\alpha \sim 0$, or $p \sim 1$, in reasonable agreement with the value of p derived from Equation (13.27) or (13.28).

The greatest theoretical difficulty in interpreting the observations of variable compact radio sources in terms of conventional synchrotron models comes from the excessively high brightness temperatures implied from the observations of rapid variations. The problem arises because causality arguments require that if variability is observed on a time scale τ , then the dimensions of the radiating region must be less than $c\tau$, since otherwise differential signal travel time over the source would blur any variations. Using the distance obtained from the redshift, z , an upper limit to the angular size, θ , may be calculated. This value of θ often leads to brightness temperatures well in excess of 10^{12} K, in apparent conflict with the maximum value allowed for an incoherent synchrotron source, particularly for variability observed

at frequencies $\nu < 1$ GHz or on time scales $t \ll 1$ year (e.g., Jones and Burbidge 1973).

For some years the variability observed at very low frequencies aroused considerable speculation about the reality of the observations, or about the validity of accepting quasar redshifts as a measure of distance. It now appears, however, that the low-frequency variations are most easily interpreted as the result of scintillations in the ionized interstellar medium (Shapirovs kaya 1978, Rickett et al. 1984). The very rapid variations observed at centimeter wavelengths, with time scales of the order of one day (Heeschen 1984), are probably also unrelated to the "classical" variability and may also be due to the same scintillation phenomenon (Blandford et al. 1986).

However, causality arguments applied to the variations which occur on time scales of the order of one year at centimeter wavelengths also predict apparent brightness temperatures which often exceed the inverse Compton limit by a factor of 10 to 100, as well as an X-ray flux which is many orders of magnitude above the values actually observed. Shortly after the implication of inverse Compton scattering was first appreciated (e.g., Hoyle et al. 1966), it was realized that the problem could be avoided if the source of radiation was moving toward the observer with a velocity close to the speed of light (Rees 1966). In this case, the apparent time scale seen by an observer at rest is shortened and the apparent brightness temperature is enhanced by "Doppler boosting." Support for the so-called "relativistic beaming" model comes from the very long baseline (VLBI) observations of "superluminal" radio sources discussed in [Section 13.3.7](#).

13.3.6. Source Dynamics and Superluminal Motion

Not unexpectedly, the compact variable radio sources show changes in their angular structure on time scales corresponding to the intensity variations: The observed motions can usually be described as an increase in separation between the core and one or more components which make up the jetlike feature. Of those sources which have been studied in any detail over a period of time, well over half show an apparent velocity of separation which appears to be five to ten times the speed of light (e.g., Cohen and Unwin 1984). This phenomenon is usually referred to as *superluminal motion*. In fact, there are very few sources where it has been clearly established that the transverse velocity is less than the speed of light. For one of these, the nucleus of [NGC 1275 \(3C84\)](#), there is a well-established subluminal motion with an apparent transverse velocity of about half the speed of light (Romney et al. 1984). [NGC 1275](#) shows the same core jet morphology seen in the superluminal sources. One of the most intensively observed superluminal sources is [3C273](#), shown in [Figure 13.7](#).

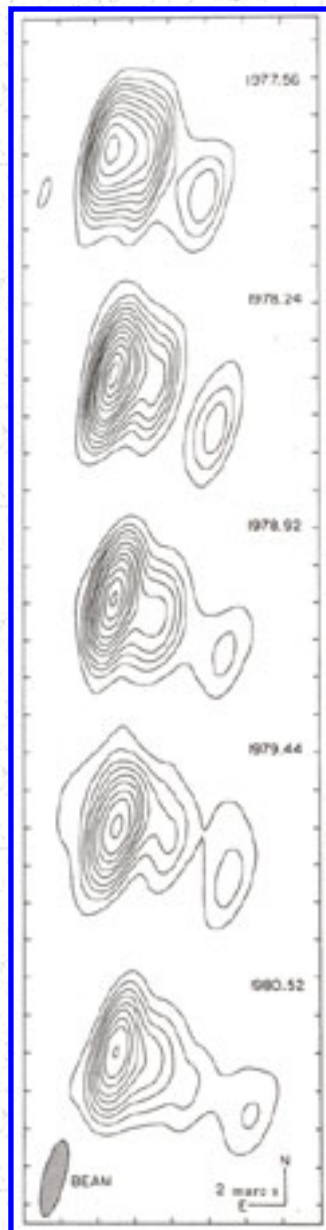


Figure 13.7. Changes in the structure of the quasar 3C273 observed between 1977 and 1981 (Pearson et al. 1981. Reprinted by permission from Nature, Vol. 290, No. 5805, pp. 365. Copyright (c) 1981, Macmillan Magazines Ltd.)

For some years there was considerable debate about whether to take the observations of superluminal motion seriously. Today the situation is very much improved. Multielement interferometer systems are used together with sophisticated image-restoring algorithms, and there is now little doubt about the reality of superluminal motion. The observed properties of the superluminal sources may be summarized as follows (e.g., Cohen and Unwin 1984, Kellermann 1985):

1. Superluminal motion is observed primarily in asymmetric sources with extended jet features and a strong core. Most are identified with bright quasars, but a few with relatively nearby AGNs.

2. Only increases in overall separations are observed, never decreases. However, in several sources there are both stationary and moving components, and in these sources, the separation of some component pairs may decrease.
3. Typical transverse velocities are of the order of $4c$ to $10c$ (e.g., [Figure 13.7](#)).
4. Component separations are typically in the range of 10 to 50 pc.
5. The cores superluminal sources show "flat" or inverted radio spectra and variable flux densities. Since the core features are more opaque than the moving components, they have flatter or more inverted spectra and are more prominent at shorter wavelengths.
6. Close to the core, the structure is often curved through an angle of several tens of degrees or more.
7. In many cases, large-scale jets also extend hundreds of kiloparsecs from the core and are continuous with the much smaller superluminal features. These large-scale jets always lie on the same side of the core as the superluminal features.
8. Different components in the same source may show different velocities. The individual components fade with time and their spectra steepen as they move away from the core.
9. In general, each component moves with a constant velocity, although there is evidence in the quasar [3C345](#) that one component has accelerated.
10. The motion is generally radial, except possibly in [3C345](#) where either the origin is displaced from the core or the direction of motion has changed.
11. Extrapolation back to the time of zero component separation often coincides with the beginning of a flux density outburst.

The observations of course give only the angular separation and its rate of change. The linear velocity is calculated from $v = R(d\theta / dt)(1 + z)$ where R is the "angular size" distance and the factor $(1 + z)$ corrects for the relativistic time dilation due to the cosmological redshift. It has been argued that if the quasars are much closer than indicated by their redshift, then of course the linear velocities may be less than c . Moreover, the apparent inverse Compton catastrophe implied by the rapid flux density variations is then no longer a problem. However, this argument does not effect the discrepancy between the observed inverse Compton flux and the distance-independent value predicted from Equation (13.20) and the measured brightness temperature (e.g., Marscher 1983).

At least one superluminal source, the AGN [3C120](#), is found in a relatively low redshift galaxy ($z = 0.03$).

Several others are identified with quasars associated with nebulosities which have measured redshifts; thus, interpretations based on noncosmological redshifts appear unsatisfactory unless noncosmological redshifts are accepted for galaxies as well as quasars.

Many models have been considered to explain superluminal motion including:

1. Appropriately phased intensity variations in fixed components-the so-called "Christmas Tree" or "Movie Marquee" model.
2. Noncosmological redshifts.
3. Gravitational lenses or screens.
4. Variations in synchrotron opacity.
5. Synchrotron curvature radiation in a dipole magnetic field.
6. Light echoes.
7. Real tachyonic motion.
8. Geometric effects of relativistically moving sources.
9. Bulk relativistic motion along the line of sight.

For one reason or another, all but the last of these have been shown to be unsatisfactory (e.g., Marscher and Scott 1980) and most of the discussion in the literature centers around models based on bulk relativistic motion. 13.3.7. Relativistic Beaming

If the source of radio emission is moving near the speed of light along a direction which lies close to the line of sight, then the source nearly catches up with its own radiation. This can give the illusion of apparent transverse motion which is greater than the speed of light. As shown in [Figure 13.8](#), if the true velocity is v and is at an angle, θ , with respect to the line of sight, then the apparent transverse velocity, v_a is given by

$$v_a = \frac{v \sin \theta}{1 - \beta \cos \theta} \quad (13.29)$$

where $\beta = v / c$.

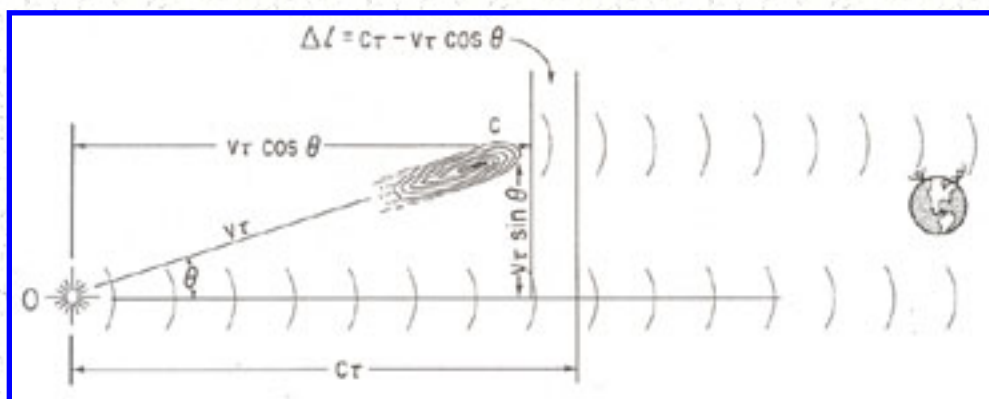


Figure 13.8. Apparent superluminal motion results when the radiating source is moving so fast that it nearly catches up with its own radiation. Assume that a radiating plasma cloud is ejected from the origin, O , with a velocity v in a direction θ with respect to the line of sight. After a time t , the cloud has moved a distance vt . The motion, projected along the line of sight is $vt \cos\theta$, and projected perpendicular to the line of sight, $vt \sin\theta$. A distant observer sees the emission delayed by a time $t(c - v \cos\theta) = ct(1 - \beta \cos\theta)$ compared to the "signal" radiated when the cloud was at O . The apparent transverse velocity seen by the observer is then $(vt \sin\theta) / [ct(1 - \beta \cos\theta)] = \beta \sin\theta / (1 - \beta \cos\theta)$.

The apparent transverse velocity has a maximum value $v_m \sim \gamma c$, which occurs at an angle $\theta = \sin^{-1}(1 / \gamma)$, where $\gamma = (1 - \beta^2)^{-1/2}$.

The Doppler shift due to the motion of the source is given by

$$\delta = \gamma^{-1}(1 - \beta \cos\theta)^{-1}. \quad (13.30)$$

If account is taken of the cosmological redshift, z , the total Doppler shift is $\delta / (1 + z)$. The observed radiation from a relativistically moving body is enhanced by an amount $[\gamma\alpha^{-3}(1 - \beta \cos\theta)]\alpha^{-3}$, which is often referred to as "Doppler boosting." For $\gamma \gg 1$, the radiation is concentrated within a small cone of half-width $\sim 1 / \gamma$. When $\theta \sim \sin^{-1}(1 / \gamma)$ (i.e., $v_a \sim v_m$), then for $\alpha \sim 0$, $\delta \sim \gamma$ and the observed emission is enhanced by a factor of $\sim \gamma^3$. The relation of the observed quantities v_a and δ and θ is conveniently represented by the diagram shown in [Figure 13.9](#).

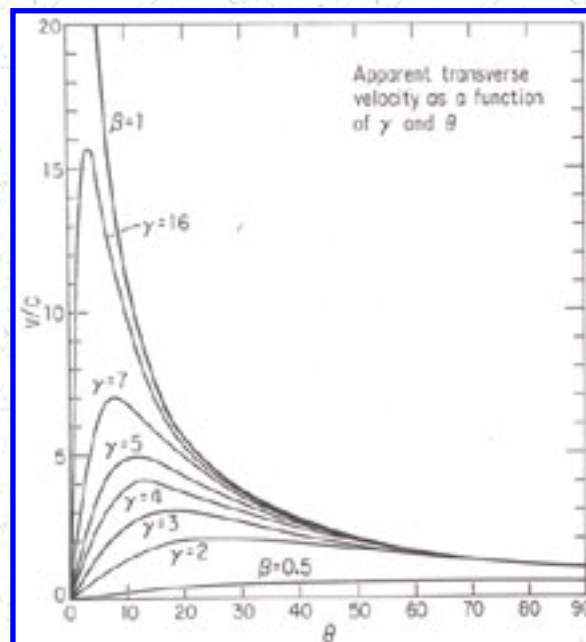


Figure 13.9. Apparent transverse velocity as a function of the Lorentz factor, γ , and the inclination to the line of sight, θ .

For an approaching component viewed "head on," the boosting factor is about $8\gamma^3$, while the receding component ($\cos \theta \sim -1$) is suppressed by a factor about $1/8 \gamma^3$ and is essentially invisible. The probability that a randomly oriented source is beamed toward the observer within an angle $\theta \sim 1/\gamma$ is $\sim 1/2 \gamma^2$ for $\gamma \gg 1$.

For values of $\gamma \sim 7$, only about one percent of a randomly oriented sample is expected to show superluminal motion, yet the observed fraction is well over one-half. The large fraction of core-dominated sources with superluminal motion can be rationalized as the result of differential Doppler boosting which preferentially selects sources with appropriate geometry in flux-limited samples. Lobe-dominated sources, on the other hand, may be assumed to be randomly oriented. But, although the statistics are limited, superluminal motion in the central cores of lobe-dominated sources such as [3C179](#) (Porcas 1981) does not seem uncommon. It is possible that the relativistic outflow occurs throughout a wide cone, but we see only that portion of the cone which is moving close to the line of sight. This would give an increased probability over the canonical $1/2 \gamma^2$ of observing superluminal motion, but the good alignment of the compact and extended jets and the highly collimated appearance of the extended jets would appear to make this interpretation unlikely.

An obvious problem with the simple relativistic beaming model is that the observed component flux densities of superluminal sources are always roughly comparable, whereas the expected flux density ratio of the approaching and receding components is $\sim \gamma^6$. Even if one component is stationary, the approaching component should appear brighter by a factor of $\sim \gamma^3$ unless, fortuitously, the intrinsic component luminosities always differ by just the right amount to cancel the differential Doppler boosting.

This apparent conflict is resolved with the *twin exhaust* model of Blandford and Konigl (1979), which has been the basis of most discussion of relativistic beaming and superluminal motion. The Blandford-Konigl model postulates symmetric relativistic beams which feed the extended lobes. The receding beam is essentially invisible since its radiation is focused in a narrow cone opposite to the line of sight and is attenuated by a factor of $\sim 1/(8\gamma^3)$. Emission from the stationary core is seen at the point where the approaching relativistic flow becomes opaque, and so it appears to be Doppler boosted by the same amount as the approaching components. Superluminal motion is observed between this stationary point in the nozzle and moving shock fronts or other inhomogeneities in the relativistic outflow. In the one source where the appropriate measurements exist, [3C345](#), the core component is indeed found to be stationary with respect to a nearby quasar (Bartel 1986).

Relativistic beaming has received considerable attention because with a minimum of assumptions it

provides a simple interpretation of

- a. superluminal motion
- b. rapid flux density variations
- c. lack of inverse Compton scattered X-rays.

In view of the apparent absence of thermal plasma in compact sources ([Section 13.3.3](#)), containing highly relativistic electrons ($\gamma \sim 1000$), the possibility of bulk relativistic motion with $\gamma \sim 10$ does not seem unreasonable.

Various "unified schemes" have been discussed which attempt to explain the difference between "core-dominated" (e.g., compact) and "lobe-dominated" (e.g., extended) sources (Orr and Browne 1982) or between "radio-loud" and radio-quiet quasars (Scheuer and Readhead 1979) as the effect of Doppler boosting of a randomly oriented parent population which causes a wide range in apparent core strength depending primarily on the orientation of the motion. However, as discussed in [Section 13.4.1](#), these unified models lead to problems with understanding the extended radio structure and large-scale one-sided radio jets, as well as the optical and X-ray emission.

The correlation between the compact radio emission and X-ray (Owen et al. 1981), infrared, and optical continuum emission suggests that if the radio emission is Doppler boosted, the continuum emission throughout the spectrum may be similarly enhanced (Konigl 1981). In many ways this would be attractive since it provides a convenient interpretation of the large dispersion in the luminosity of quasars which appear to be up to about 5 magnitudes brighter than first-ranked elliptical galaxies. But if the strength of the optical continuum depends primarily on geometry, it is difficult to understand the small spread in the ratio of emission line to continuum brightness, since the line-emitting regions do not show large blue shifts (e.g., Heckman et al. 1983b).

The trivial ballistic model described above is surely too simple. If the actual motion is in the form of a continuous flow rather than the motion of discrete components, then the Doppler boosting factor $\delta = [\gamma\alpha^{-2}(1 - \beta^2)]\alpha^{-2}$. More generally, Lind and Blandford (1985) have emphasized that the actual flow velocity may differ from the shock front velocity, which may be moving obliquely to the main flow. Since it is the relativistic flow velocity which causes the Doppler boosting and the shock front velocity which is seen as superluminal motion, the apparent constraints discussed above may be relaxed. However, in the one object where there is a direct Doppler measure of the flow velocity, SS433 (see Chapter 9), it is equal to the measured radio component velocity.

Realistic models will also be affected by variations in the opacity and dispersion in the actual velocity γ and in the intrinsic radio luminosity. Attempts to explain the wide range of properties of compact AGNs and quasars as simply geometric effects are probably unrealistic, but there is good evidence that the effect of relativistic beaming is relevant to quasars and AGNs, at least at radio wavelengths.

The importance of relativistic beaming and Doppler boosting of the radio, optical, infrared, and X-ray

continuum is one of the central problems of current extragalactic research and may have profound implications for our understanding of quasars and AGNs.

13.4. EXTENDED SOURCES

During the 1950s and 1960s, the imaging of extragalactic radio sources steadily improved, and most resolved sources appeared to be simple double sources surrounding either an optical galaxy or quasar. This led to theories involving explosions in the parent object which ejected clouds of magnetized plasma and relativistic particles (e.g., De Young and Axford 1967). It soon became clear however, that in the simple versions of these models, radiation and adiabatic expansion losses were too large (e.g., Scheuer 1974). Thus, some sort of continuous supply of energy and, in some cases, in situ particle acceleration were required, and an external medium surrounding the radio-emitting region appeared to be necessary to keep the source from too dispersing rapidly.

Models involving ejection of multiple blobs of plasma (or plasmons) were suggested by Christiansen (1973) and others to overcome the rapid losses. A second class of model, supported by Saslaw et al. (1974) involved the ejection of supermassive objects, via three-body interactions in the nucleus, which then supplied relativistic particles continuously to maintain the source. A third class of models, first proposed by Rees (1971) and colleagues, involved resupply of the radio lobes by a continuous beam of particles or waves.

13.4.1. Jets, Lobes, and Hot Spots

The apparently simple properties of powerful, (i.e., $L > 10^{40}$ erg s⁻¹) extragalactic radio sources have been complicated by the high-resolution maps which have become available over the past fifteen years with ever increasing detail. However, at the same time, the nature of the physical processes necessary to explain these sources have become clearer.

For some time it has been clear that a general description of an "extragalactic source" includes a central component and some sort of extended double structure. During the 1980s, it has become evident that virtually all such sources also have narrow elongated tubes of radio emission connecting the central source to the outlying extended structure, suggesting that energy, magnetic field, relativistic particles, and probably thermal gas are being transferred away from the nucleus to form the observed extended structures.

The detailed morphology illustrated in [Figure 13.10](#) has resulted in an updated form of the Rees (1971) beam model being generally accepted as the working picture of extragalactic radio sources. The models of Rees envisioned an invisible, relativistic flow which terminated in a shock where the flow energy was randomized and emerged, at least partly, as the flux of relativistic particles necessary to maintain the extended emission. Unlike the original model, however, the radio jets now commonly observed, emit radiation. Thus, the transport process must not be entirely efficient. Also many jets are observed to bend and wiggle, probably indicating an interaction with an external medium. In nearby sources, this medium

is often observed through its X-ray emission and appears to be in pressure equilibrium with the plasma in the jet. Properties of radio jets are discussed more fully by Bridle and Perley (1984).

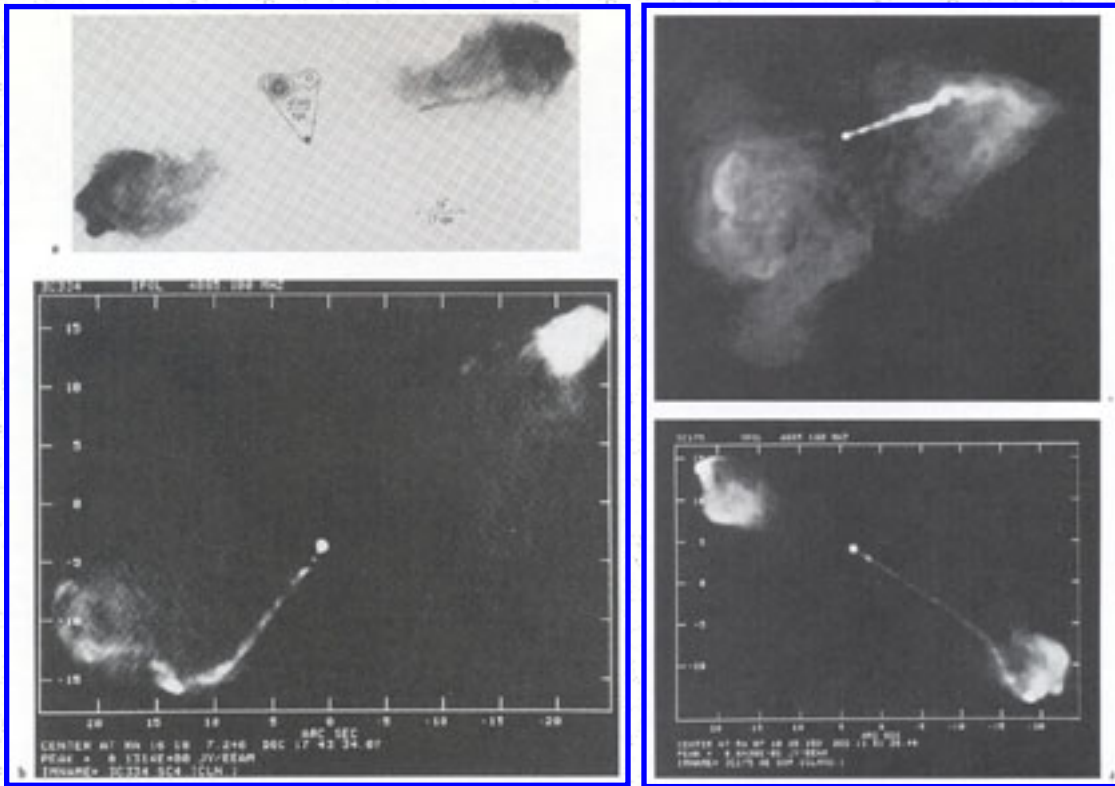


Figure 13.10. (a) [Cygnus A](#) is the strongest extragalactic radio source in the sky and is the prototypical example of FR I radio structure. The image of the extended structure was made using the VLA (From Perley et al. 1984) and shows a faint radio jet which apparently feeds the outer hot spot on one side and the filamentary radio lobes. The structure shown for the compact core is based on VLBI data (From Downes et al. 1981). (b) [3C334](#) has a curved knotty jet emanating from the bright unresolved source that coincides with the quasar. Both lobes contain some filamentary substructure. The thin filament extending back toward the quasar from the northwestern lobe may be part of a weak counterjet, which is rarely seen in powerful sources except on images of very high dynamic range. Counterjets are very common, however, in low-power sources. (Observers: Owen and Hines. Courtesy NRAO/AUI.) (c) [M87](#) is a relatively weak radio galaxy in the [Virgo cluster](#). The jet, shown here, is about 2 kpc in extent and its emission extends from the radio into the optical and X-ray regions of the spectrum. (d) The unresolved bright spot near the center of this 5GHz image is coincident with a quasar at a red shift of 0.77. The long, narrow, one sided radio jet is typical of powerful double lobed sources. There are prominent hot spots in both lobes suggesting that they have both been recently supplied with relativistic particles despite the appearance of only a single jet. (c and d: Observers: A. Bridle, I. Browne, J. Burns, J. Dreher, D. Hough, R. Laing, C.

Lonsdale, P. Scheuer, J. Wardle).

Extended extragalactic sources also show a basic change in their morphology at an absolute luminosity of $P(14 \text{ GHz}) \sim 10^{25} \text{ W Hz}^{-1}$. Sources weaker than this level appear limb darkened, that is, they slowly fade away in brightness as one looks further away from the nucleus, while brighter sources have limb-brightened outer structures. The two classes are referred to as Fanaroff and Riley (1974) classes I and II, respectively (or FR I and FR II). FR II sources also often show small "hot spots" either at the farthest edges of the source or sometimes apparently embedded in more diffuse structure. It is believed that the entire limb-brightened structure is due to supersonic jets terminating at a boundary with an external medium surrounding the source. FR I sources, on the other hand, may be subsonic, at least in their outermost regions. They are thought to be in thermal pressure balance with the external medium and possibly to have entrained a great deal of external gas. FR I sources are often found in nearby rich clusters of galaxies and are often distorted by processes in the clusters.

Because of their higher luminosity and relatively low space density, FR II sources tend to be identified with distant radio galaxies and quasars, often near the edge of the observable universe. However, some examples do exist relatively nearby, such as [Cygnus A](#) which has a redshift of 0.057. Its parent galaxy has long been known to have very strong emission lines. The galaxy is also very bright at optical wavelengths but unfortunately lies within ten degrees of the galactic plane, which makes it difficult to study optically. It lies in the center of a very dense ($n_e \sim 10^{-2} \text{ cm}^{-3}$) cloud of very hot (10^8 K) gas. Lower-luminosity examples of the class, which are more common nearby, do not generally show such extreme X-ray properties and, except for some nuclear emission lines, resemble normal giant elliptical galaxies.

The dominant morphological characteristic of FR II radio galaxy emission is the brighter outer lobes. Often embedded in the lobes are more compact hot spots, perhaps as small as one kiloparsec. This structure is usually accompanied by a compact core in the center of the galaxy, although the core is sometimes too weak to be seen with present maps. Finally, in nearby examples which have been studied very extensively with the VLA, a faint jet can be seen connecting the nucleus with the outer hot spots and lobes, at least on one side of the double. Such jets have been seen in only a few cases, and it is unclear whether the jets are strongly one-sided as in the quasars discussed below.

The general properties of this morphology have recently been convincingly reproduced in numerical simulations of low-density, supersonic jets traveling through a denser external medium. This type of work is just beginning but suggests that we are on the right track and may ultimately be able to understand a great deal about these sources.

Quasars also produce FR II sources. However, the relative importance of the distinct features of the general morphology often is different. The bright outer lobes and hot spots are still visible but the central component and the jets are much brighter, both relative to the lobes and in absolute terms. The luminosity of the central component and jet of quasars is usually one to two orders of magnitude higher than for the galaxies. Quasar jets almost always appear to be one-sided. Furthermore, these jets often show many bends and wiggles, sometimes by as much as ninety degrees. They often seem to be made up

of many small knots rather than a continuous brightness distribution.

The origin of the one-sidedness is, at present, still unclear. On the one hand, many of the properties seem consistent with relativistic beaming in the line of sight, as is used to explain the observed compact jets ([Section 13.3.7](#)). The ratio of brightness from one side to the other in any given case is consistent with fairly small values of γ 's. Also the pronounced wiggles and bends can be more easily understood if they are intrinsically small wiggles, which when inclined to the line of sight, appear to be large bends in projection on the sky. Moreover, where VLBI and VLA observations exist for the same source, the one-sided jets on both scales lie on the same side of the source, suggesting a common origin for the observed one-sidedness.

However, it is hard to understand how this can be the case since in radio quasars we see only one-sided jets and we almost always can detect a jet. Also, quasars with one-sided jets and bright radio cores exist which appear as large as all but a few of the largest radio galaxies, so they are unlikely to be appreciably foreshortened (e.g., Schilizzi and de Bruyn 1983). Alternatively, the high-luminosity jets may be intrinsically one-sided. Since the diffuse lobe emission is usually found on both sides of the nucleus, this seems to imply that either the missing jet is not radiating as strongly for some reason or that the jet "flip-flops" between the two sides (Rudnick and Edgar 1984). Also, since there is strong evidence for relativistic motion in the core ([Section 13.3.7](#)), such a picture implies that the jet slows down a great deal on its journey to the outer lobe. Neither picture is entirely satisfactory at this time.

Both FR I and FR II sources can exhibit large degrees of linear polarization, $\gtrsim 50\%$ locally; however, the jets in the two types of sources usually show very different field geometry. Most straight FR I sources show either magnetic fields predominantly perpendicular to the jet axis or perpendicular fields which change to predominantly parallel fields at some point down the jet. Exceptions to this trend sometimes occur in very bent sources, where stretching and shearing near the bend may cause an apparent parallel-to-perpendicular flip in the magnetic field. In FR II sources, the magnetic field is usually parallel to the jet axis all the way along the radio jet. The lobes of FR II sources, however, usually have the magnetic field running along the outer edge of the lobe.

The lower-luminosity FR I sources which have been studied up to now are much more nearby on average, and thus we know more about the environment in which they exist. Virtually all are found in some sort of galaxy clustering from poor groups up to the richest clusters. In many of these cases, especially in rich clusters, we know from X-ray observations that they are surrounded by a hot (10^7 to 10^8 K), relatively dense (10^{-2} to 10^{-4} cm^{-3}) medium. The pressures inside the radio sources implied by minimum-energy calculations are often equal to or less than the pressure of the external hot medium. This relationship plus the relaxed-looking, distorted nature of FR I sources suggests that the interaction with the external medium is extremely important in determining the properties of these sources.

FR I sources take on a variety of morphological shapes. However, some general patterns can be recognized. The most luminous FR I sources are usually associated with bright D or cD galaxies located in the center of their associated cluster. They are usually one or two magnitudes brighter than the giant

elliptical galaxies usually associated with (nearby) FR II sources. These galaxies also usually have a less rapidly dropping light distribution, suggesting a flatter gravitational potential of much larger extent than is found for the FR II sources. Their radio morphology can usually be described as a twin jet with a gradually widening and often bending channel. Many of these sources, especially those in rich clusters, are bent into C-shapes. These sources are called *wide-angle tails*.

At lower luminosities in rich clusters, one often finds sources which have apparently been even more distorted with jets which have been bent by ninety degrees on each side of the galaxy and merge into long diffuse tails. These sources are called *narrow-angle tails*. Their parent galaxies are intermediate in optical luminosity between *wide-angle tails* galaxies and FR II sources. They are believed to be formed by a normal radio galaxy moving through the hot, tenuous medium in a cluster (e.g., Owen et al. 1979), although this may be hard to reconcile with the very longest-tailed sources (Burns 1981).

Almost all FR I sources have a prominent central component, although this is mainly due to the lower surface brightness of the extended emission compared with FR II sources. Most show two-sided jets. These jets are often close to being equal in brightness, and in a few cases the orientation of dust lanes actually suggests that the slightly brighter jet is pointed away from us. Thus, relativistic motion is not indicated for these sources, at least far away from the nucleus.

13.4.2. Jet Physics

Since we have no direct way of estimating the density and velocity of a radio-emitting jet, a maze of indirect arguments and physical assumptions is made to deduce the nature of the phenomena. However, within the framework of a set of physical assumptions, many deductions can be made, and if we do not make a completely incorrect assumption, (for example, that the radio brightness is due to the incoherent synchrotron process), we can sometimes limit the physical conditions to a fairly narrow range of possibilities. Basically, we have the radio brightness and its linear polarization at one or more frequencies to work with. We also may have some knowledge of the external conditions from X-ray or optical observations.

(a) Straight Jets

Let us assume that a jet is a collimated flow consisting of thermal and relativistic gas initially moving with some velocity v and some radius r . The brightness is then affected by (1) radiation losses, (2) adiabatic gains or losses, and (3) other energy gains or losses by the relativistic electrons. As a jet expands, the particles in the jet will gain or lose energy, consistent with their equation of state. In particular, the relativistic particle energy density, ϵ , in a volume V will change as $\epsilon \propto V^{-4/3}$, or the the total energy of a single particle will vary as $E \propto V^{-1/3}$.

Thus, in the cylindrical geometry of a jet, as the radius of the jet, r_j , increases, each relativistic electron should lose energy to the expansion as $E \propto r_j^{-2/9}$.

If magnetic flux is conserved then $B_{\parallel} \propto r_j^{-1}$, and $B_{\perp} \propto r_j^{-2}$.

If the velocity of the jet, v_j , remains constant and no energy is added to the particles or magnetic field from other sources, the luminosity of all observed jets would decrease much faster than is observed (e.g., Bridle and Perley 1984). Thus one of these assumptions must be incorrect. If the velocity decreases, then the density of particles and the perpendicular magnetic field strength will increase, thus counteracting the effects of any expansion. Combining both effects for a power law energy spectrum, the intensity, I_{ν} varies as

$$I_{\nu} \propto r_j^{-(5p+4)/3} v_j^{-(p+2)/3} \quad (B_{\parallel})$$

or

$$I_{\nu} \propto r_j^{-(7p+5)/6} v_j^{-(5p+7)/6} \quad (B_{\perp})$$

Thus, the jet can actually brighten with certain combinations of parameters. However, if v_j decreases sufficiently, then radiation losses can become important. Also, particles lose energy through inverse Compton scattering to the 3 K background, so the net rate at which particles lose energy reaches a minimum at a magnetic field strength of a few microgauss. Thus, it is not possible to explain the brightness of jets by simply letting v decrease indefinitely. If adiabatic effects alone cannot explain the brightness distribution, then some nonadiabatic effect must be contributing to the energy in the particles and/or fields. The most obvious source is probably the energy in the bulk flow of any thermal plasma in the jet. This could be transferred to the particles through interactions with shocks or through plasma waves in a turbulent plasma. These processes, however, seem to work best when adding energy to already relativistic particles. Theoretical calculations and in situ space observations show they are very inefficient in accelerating thermal particles, especially electrons, to relativistic energies (Lee 1983). Since these and other processes are uncertain in their details, usually it is simply assumed that a fraction, η , of the kinetic energy in the jet is converted to relativistic electron energy. Thus,

$$L_{\text{rad}} = \frac{1}{2\eta r_j \rho_j v_j^3} \quad (13.31)$$

where L_{rad} is the total emitted radiation and ρ_j is the density of thermal particles in the jet.

Equation (13.31) is called the kinetic luminosity equation. Rough estimates for jet or total-source requirements are often made by simply using the total luminosity of (half) of the source as L_{rad} and estimating ρ from the observed Faraday depolarization or the density of the background gas. Clearly, a better approach would be to combine at least adiabatic effects with particle acceleration but this has rarely been done.

(b) Bent Jets

If as in the wide-angle tails or narrow-angle tails, the jet is bent, an additional constraint exists, since the time-independent Euler's equation should apply or

$$(v \cdot \nabla)v = \frac{1}{\rho} \nabla P. \quad (13.32)$$

If R is the scale length over the jet bends, then $(v \cdot \nabla)v \simeq v_b^2 / R$. Then

$$\frac{\rho_j v_j^2}{R} \simeq \nabla P. \quad (13.33)$$

A galaxy moving with velocity v_g through an intracluster medium with density ρ_{icm} experiences a ram pressure $\rho_{\text{icm}} v_g^2$. This pressure is exerted over a scale length h . If the jet is directly exposed to the intracluster medium, then $h = r_j$. On the other hand, the jet maybe inside the interstellar medium of a galaxy. Then h is the pressure scale height in the galaxy. In any case, one can write

$$\frac{\rho_j v_j^2}{R} \simeq \frac{\rho_{\text{icm}} v_g^2}{h}. \quad (13.34)$$

Combining the kinetic luminosity equation (13.31) with the Euler's equation in the form (13.32), we can eliminate one of the common variables. For example, eliminating v_b we can get

$$v_g = \left[\frac{2\rho_j^{1/2} L_{\text{rad}} (r_j/R)^{3/2}}{\pi r_j^2 \eta \rho_{\text{icm}}^{3/2}} \right]^{1/3}. \quad (13.35)$$

For cases involving narrow-angle tails moving at 10^3 km s^{-1} with respect to the external medium, one can find acceptable applications of this equation. However, for the wide-angle tails, one has a higher luminosity to explain and strong evidence in some cases that the parent galaxy is moving very slowly or not at all with respect to the intracluster medium. Thus, a simple picture of motion causing the bending of wide-angle tails appears to fail. More complete models including adiabatic effects or other energy sources for the particles such as turbulence in the gas entrained from the intracluster medium appear to be necessary.

5. SUMMARY

There is convincing quantitative evidence that all of the extragalactic radio sources radiate by the commonly accepted incoherent synchrotron process. This evidence includes:

1. The shapes of the spectra of the extended (transparent) sources are power law or dual power law and their detailed shapes are in agreement with synchrotron models where the relativistic particles both gain and lose energy.
2. In the compact sources, the spectral peak occurs at shorter wavelengths in the smaller sources, as predicted by the synchrotron model, and the measured angular sizes are in good agreement with those estimated from the observed self-absorption cutoff wavelength.
3. The maximum observed brightness temperature is $\sim 10^{12}$, as is expected from an incoherent synchrotron source which is "cooled" by inverse Compton scattering.
4. The variations in intensity and polarization and their dependence on wavelength and time are in qualitative agreement with those expected from an expanding cloud of relativistic particles.

The source of energy, the so-called "central engine," is thought to be the associated quasar or AGN. The observed correlation between 21-cm observations of HI and the strength of the nuclear radio source supports the concept that the radio source is fueled by the accretion of gas onto a massive collapsed object, possibly a black hole.

Energy from the central engine appears to be transported to the outer lobes via a highly collimated beam of relativistic particles, but there has been little progress in understanding how the potential energy of the condensed object is converted into an apparently stable particle beam. Near the core, VLBI measurements, as well as observations of rapid flux density variations and the absence of inverse Compton scattered X-rays, are interpreted as the result of Doppler beaming by a highly relativistic outflow from the nucleus with Lorentz factors typically in the range of 5 to 10. But the evidence for bulk relativistic motion in the extended jets is ambiguous.

Recommended Reading

1. Begelman, M.C., R.D. Blandford, and M.J. Rees. 1984. *Rev. Mod. Phys.* 56:225.
2. Bridle, A.H., and R.A. Perley. 1984. *Annu. Rev. Astron. Astrophys.* 22:319.
3. De Young, D.S. 1984. *Physics Reports* 111:373.
4. Dyson, J.E. (ed.). 1985. *Active Galactic Nuclei*. Manchester: University of Manchester Press.
5. Fanti, R., K.I. Kellermann, and G. Setti. (eds.). 1984. *IAU Symposium No. 110, VLBI and Compact Radio Sources*. Dordrecht: Reidel.
6. Heeschen; D.S., and C.M. Wade. (eds.). 1982. *IAU Symposium No. 97, Extragalactic Radio Sources*. Dordrecht: Reidel.
7. Kellermann, K.I., and I.I.K. Pauliny-Toth. 1981. *Annu. Rev. Astron. Astrophys.* 19:410.
8. Moffet, A.1975. In A. Sandage, M. Sandage, J. Kristian. (eds.), *Stars and Stellar Systems*, Vol. 9.

Chicago: University of Chicago Press, p. 211.

9. Swarup, G., and V.K. Kapahi. 1986. IAU Symposium No. 119, Quasars. Dordrecht: Reidel.
10. Zensus, J.A. and S. Unwin. (eds.). 1987. Superluminal Radio Sources. Cambridge: Cambridge University Press.

REFERENCES

1. Aller, H.D., M.F. Aller, G.E. Latimer, and P.E. Hodge. 1985. *Astrophys. J. Suppl.* 59:513.
2. Altschuler, D.R., and J.F.C. Wardle. 1977. *Mon. Not. R. Astron. Soc.* 179:153.
3. Andrew, B.H., J.M. MacLeod, G.A. Harvey, and W.J. Meade. 1978. *Astron. J.* 83:863.
4. Baade, W. and R. Minkowski. 1954. *Astrophys. J.* 119:206.
5. Bartel, N. 1986. *Nature* 319:733.
6. Begelman, M.C., R.D. Blandford, and M.J. Rees. 1984. *Rev. Mod. Phys.* 56:255.
7. Bicknell, G.V. 1986. *Astrophys. J.* 300:591.
8. Biermann, P., and J.A. Zensus. 1984. In W. Brinkmann and J. Trumper (eds.), *Proceedings of Conference on X-ray and UV Emission from Active Galactic Nuclei*. Garching: Max Planck Institute für Extraterrestrische Physik, p. 275.
9. Biretta, J.A., F.N. Owen, and P.E. Hardee. 1983a. *Astrophys. J. (Lett.)* 274:L27.
10. Biretta, J.A., M.H. Cohen, S.C. Unwin, and I.I.K. Pauliny-Toth. 1983b. *Nature* 306:42.
11. Blandford, R.D., R. Narayan, and R.W. Romani. 1986. *Astrophys. J. (Lett.)* 301:L53.
12. Blandford, R., and A. Konigl. 1979. *Astrophys. J.* 232:34.
13. Bolton, J., and G.J. Stanley. 1949. *Aust. J. Sci. Res.* 2A:139.
14. Bregman, J.N., A.E. Glassgold, P.J. Huggins, G. Neugebauer, B.T. Soiffer, K. Matthews, J. Elias, J. Webb, J.T. Pollock, A.J. Pica, R.J. Leacock, A.G. Smith, H.O. Aller, M.F. Aller, P.E., Hodge, W.A. Dent, T.J. Bulonek, R.E. Barvanis, T.P.L. Roellig, W.Z. Wisniewski, G.H. Bieke, M.J. Lebofsky, B.J. Wills, D. Wills, W.H.-M. Ku, J.D. Bregman, F.C. Witteborn, D.F. Lester, C.D. Impey, and J.A. Hackwell. 1986. *Astrophys. J.* 301:708.
15. Burns, J.O. 1981. *Mon. Not. R. Astron. Soc.* 196:523.
16. Christiansen, W.A. 1973. *Mon. Not. R. Astron. Soc.* 164:211.
17. Cohen, M., and S.C. Unwin. 1984. In R. Fanti et al. (eds.), *Proceedings of IAU Symposium 110, VLBI and Compact Radio Sources*. Dordrecht: Reidel, p. 95.
18. Condon, J.J. 1982. *Astrophys. J.* 252:102.
19. Condon, J.J., and A. Dressel. 1973. *Astrophys. Lett.* 15:203.
20. de Bruyn, G. 1976. *Astron. Astrophys.* 52:439.
21. Dent, W.A. et al. 1974. *Astron. J.* 79:1232.
22. Dent, W.A., and J.E. Kapitsky. 1976. *Astron. J.* 81:1053.
23. De Young, D.S. 1984. *Physics Reports* 111:373.
24. De Young, D.S., and W.I. Axford. 1967. *Nature* 216:129.
25. Downes, A., et al. 1981. *Astron. Astrophys.* 97:L1.
26. Dreher, J.W., C.C. Carilli, and R.A. Perley. 1987. *Astrophys. J.* 316:611.
27. Dressel, A., and J.J. Condon. 1978. *Astrophys. J. Suppl.* 36:53.
28. Ekers, R.D. 1978. *Phys. Scripta* 17:171.
29. Ekers, R.D. 1981. In S.M. Fall and D. Lynden-Bell (eds.), *Structure and Evolution of Normal*

- Galaxies Cambridge, England: Cambridge University Press, p. 169.
30. Ennis, D.J., G. Neugebauer, and M. Werner. 1982. *Astrophys. J.* 262:460.
 31. Epstein, E.E., W.G. Fogarty, J. Mottmann, E. Schneider. 1982. *Astron. J.* 87:449.
 32. Fanaroff, B.L., and J.M. Riley. 1974. *Mon. Not. R. Astron. Sci.* 167:31.
 33. Fanti, C., R. Fanti, F. Ficarra, F. Mantovani, L. Padvielli, and K. Weiler. 1981. *Astron. Astrophys. Suppl.* 45:61.
 34. Fanti, C., R. Fanti, A. Ficarra, L. Gregorini, F. Mantovani, and L. Padvielli. 1983. *Astron. Astrophys. Suppl.* 118:171.
 35. Hazard, C., M.B. Mackey, and A.J. Shimmins. 1963. *Nature* 197:1037.
 36. Heckman, T.M., W. Van Brengel, G.K. Mcley, and H.R. Butcher. 1983a. *Astron. J.* 88:1077.
 37. Heckman, T.M. 1983b. *Astrophys. J.* 271:L5.
 38. Heeschen, D.S. 1984. *Astron. J.* 89:1111.
 39. Hey, J.S., S.J. Parsons, and J.W. Phillips. 1946. *Nature* 158:234.
 40. Hoyle, F., G. Burbidge, and W. Sargent. 1966. *Nature* 209:751.
 41. Hummel, K. 1980. *Astron. Astrophys. Suppl.* 41:151.
 42. Jones, T.W., and G.R. Burbidge. 1973. *Astrophys. J.* 186:791.
 43. Jones, T.W., and S.L. O'Dell. 1977. *Astron. Astrophys.* 61:291.
 44. Jones, T.W., S.L. O'Dell, and W.A. Stein. 1974a. *Astrophys. J.* 188:353.
 45. Jones, T.W., S.L. O'Dell, and W.A. Stein. 1974b. *Astrophys. J.* 192:261.
 46. Jones, D.L.; J.M. Wrobel, and D.B. Shoffer. 1984. *Astrophys. J.* 276:480.
 47. Kardashev, N.S. 1962. *Sov. Astron: AJ* 6:317.
 48. Kellermann, K.I. 1985. *Comments Astrophys.* 11:69.
 49. Kellermann, K.I., and I.I.K. Pauliny-loth. 1968. *Ann. Rev. Astron. Astrophys.* 6:417.
 50. Konigl, A. 1981. *Astrophys. J.* 243:700.
 51. Kotanyi, C.G. 1980. *Astron. Astrophys. Suppl.* 41:421.
 52. Kronberg, P.P., P. Biermann, and F.R. Schwab. 1981. *Astrophys. J.* 246:751.
 53. Landau, R., T.W. Jones, E.E. Epstein, G. Neugebauer, B.T., Soifer, M.W. Werner, J.J. Puschell, and T.J. Balonek. 1983. *Astrophys. J.* 268:68.
 54. Lee, M.A. 1983. *Rev. Geophys. Space Phys.* 21:324.
 55. Lind, K.R., and R.D. Blandford. 1985. *Nature* 314:424.
 56. Marcaide, J.M., N. Bartel, M.V. Gorenstein, LL Shopiro, B.E. Corey, A.E.E. Rogers, J.C. Webber, T.A. Clark, J.D. Romney, and R.A. Preston. 1985. *Nature* 314:424.
 57. Marscher, A.P. 1983. *Astrophys. J.* 264:296.
 58. Marscher, A.P., and J.S. Scott. 1980. *Publ. Astron. Soc. Pacific* 92:127.
 59. Meurs, E.J.A., and A. Wilson. 1984. *Astron. Astrophys.* 136:206.
 60. Miley, G. 1980. *Annu. Rev. Astron. Astrophys.* 18:165.
 61. Minkowski, R. 1960. *Astrophys. J.* 132:908.
 62. Moffet, A. 1975. In A. Sandage, M. Sandage, and J. Kristian (eds.), *Stars and Stellar Systems*, Vol. 9. Chicago: University of Chicago Press, p. 211.
 63. Orr, M.J.L.; and I.W.A. Browne. 1982. *Mon. Not. R. Astron. Soc.* 200:1067.
 64. Owen, F., J.O. Burns, L. Rudnick, and E.W. Greisen. 1979. *Astrophys. J. (Lett.)* 229:L59.
 65. Owen, F., D. Helfand, and S.R. Spangler. 1981. *Astrophys. J. (Lett.)* 250:L55.
 66. Owen, F.N., and J.J. Puschell. 1984. *Astron. J.* 89:932.

67. Pearson, T.J., S.C. Unwin, M.H. Cohen, R. Linfield, A.C.S. Readhead, G.A. Seielstad, R.S. Simon, and R.C. Walker. 1981. *Nature* 290:365.
68. Perley, R.A., J.W. Dreher, and J. Cowan. 1984. *Astrophys. J.* 285:L35.
69. Peterson, F.W., and W.A. Dent, 1973. *Astrophys. J.* 186:421.
70. Porcas, R.W. 1981. *Nature* 294:47.
71. Preuss, E., W. Alef, and A. Pedlor. 1987. In K. Fricke (ed.), *Observational Evidence of Activity in Galaxies Proceedings of IAU Symposium No. 121*. Dordrecht: Reidel, p. 269.
72. Rees, M.J. 1966. *Nature* 211:468.
73. Rees, M.J. 1971. *Nature* 229:312.
74. Rickett, B.J., W.A. Coles, and G. Bourgois. 1984. *Astron. Astrophys.* 134:390.
75. Roellig, T.L., et al. 1986. *Astrophys. J.* 304:646.
76. Romney, J., et al. 1984. In R. Fanti et al. (eds.), *IAU Symposium 110, VLBI and Compact Radio Sources*. Dordrecht: Reidel, p. 137.
77. Rudnick, L., and B.K. Edgar. 1984. *Astrophys. J.* 279:74.
78. Sadler, E. 1984. *Astron. J.* 89:53.
79. Saslaw, W.C., M.J. Valtoner, and S.J. Anrseth. 1974. *Astrophys. J.* 190:253.
80. Scheuer, P.A.G. 1974. *Mon. Not. R. Astron. Soc.* 166:513.
81. Scheuer, P.A.G., and A.C.S. Readhead. 1979. *Nature* 277:182.
82. Schilizzi, R.T., and A.G. de Bruyn. 1983. *Nature* 303:26.
83. Schmidt, M. 1963. *Nature* 197:1040.
84. Sciama, D.W., and M.J. Rees. 1967. *Nature* 216:147.
85. Shapirovskaya, N. Ya. 1978. *Sov. Astron.-AJ* 22:544.
86. Shklovsky, I.S. 1965. *Sov. Astron.-AJ* 9:22.
87. Smith, F.G. 1951. *Nature* 168:555.
88. Spinrad, H., et al. 1985. *Publ. Astron. Soc. Pacific* 97:932.
89. Stocke, J. 1978. *Astron. J.* 83:348.
90. van der Hulst, J.M., P.C. Crane, and W.C. Keel. 1981. *Astron. J.* 86:1175.
91. van der Laan, H. 1966. *Nature* 211:1131.
92. Walker, R.C., J.M. Benson, and S.C. Unwin. 1987. *Astrophys. J.* 316:546.
93. Wardle, J.F.C. 1977. *Nature* 269:563.
94. Wilson, A. 1982. *Highlights of Astronomy* 6:467.
95. Wolfe, A. (ed.). 1978. *Pittsburgh Conference on BL Lac Objects*. Pittsburgh, Pennsylvania: University of Pittsburgh.
96. Wrobel, J.M., and D.S. Heeschen. 1984. *Astrophys. J.* 287:41.
97. Wrobel, J.M., D.L. Jones, and D.B. Shaffer. 1985. *Astrophys. J.* 289:598.